Particle Identification

Lesson 1 - Detectors

M. Contalbrigo – INFN Ferrara

2nd European School on the Physics of the EIC and Related Topics, 22th June – 2nd July, 2025

Particle-ID Detectors based on Tracking Calorimetry	Passage through massive absorbers Kinematics Energy momentum balance Shower shape
Particle-ID Detectors as Tracking by-product	Ionization Energy Loss Transition Detection
Particle-ID Sensors	Multi-Anode Photomultipliers Micro-channel Plates Silicon Photomultipliers Low Gain Avalanche Photodiode
Specific Particle-ID Detectors	Time-of-Flight Cherenkov Radiation

PID from Tracking & Calorimetry

Tracking / Calorimetry

Process	Particle	Equipment
Passage through massive absorbers	Muons	Tracking
Kinematics (exclusive topology in decays or final state)	Hadrons	Tracking
Energy-momentum balance	Electrons / Gammas	Tracking / Calorimetry
Energy only	Neutrals	Calorimetry
Shower shape in calorimeters	Electrons / Gammas	Calorimetry

Process	Particle	Equipment
Passage through massive absorbers	Muons	Tracking

CMS

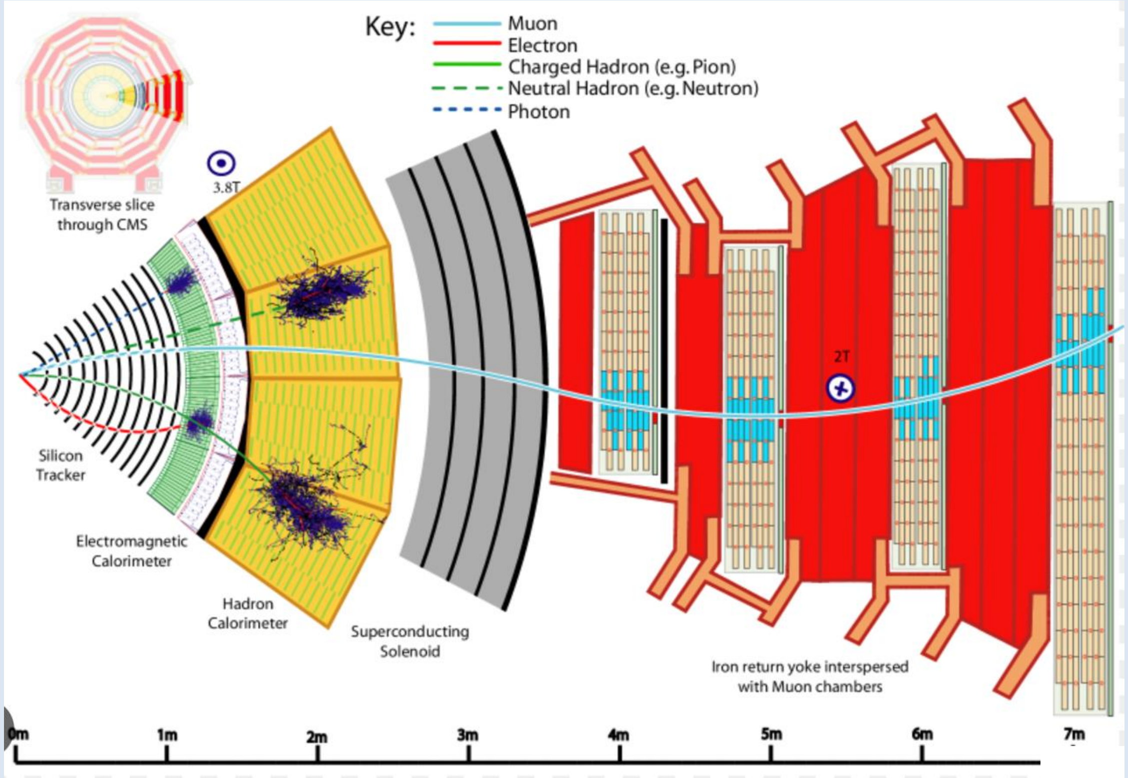

Tracking

Process	Particle	Equipment
Kinematics (exclusive topology in decays or final state)	Hadrons	Tracking

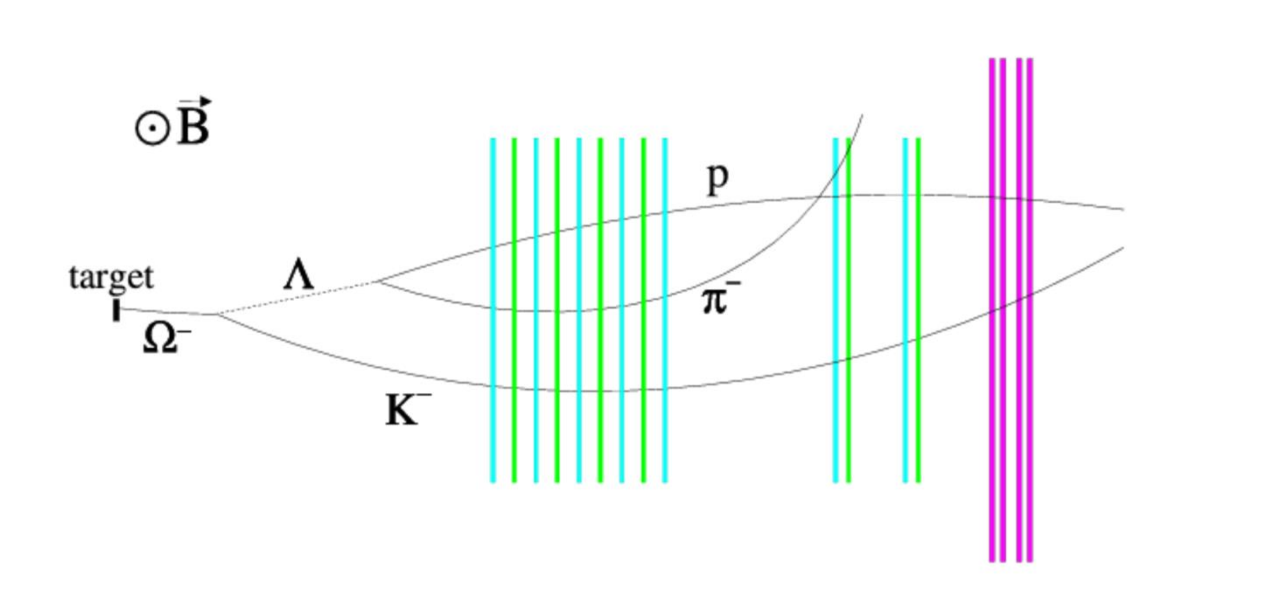

Tracking / Calorimetry

Process	Particle	Equipment
Energy-momentum balance	Electrons / Gammas	Tracking / Calorimetry

NOMAD

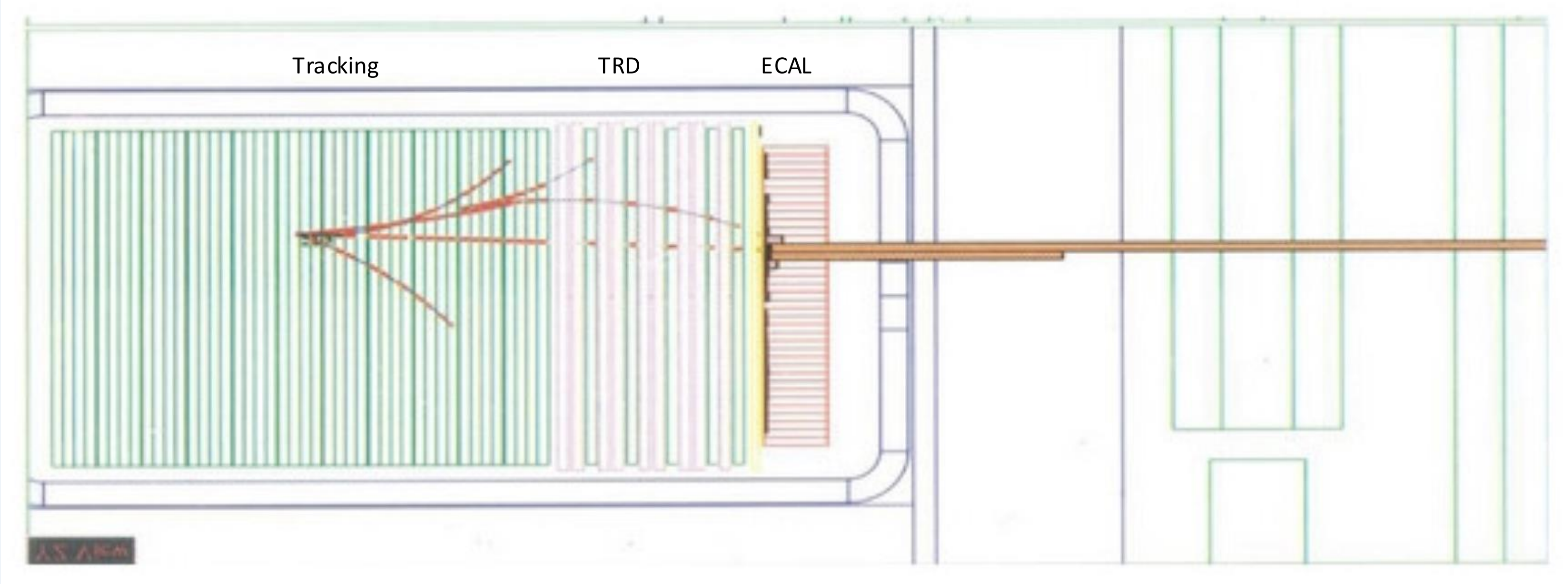

Tracking / Calorimetry

Process	Particle	Equipment
Energy only	Neutrals	Calorimetry

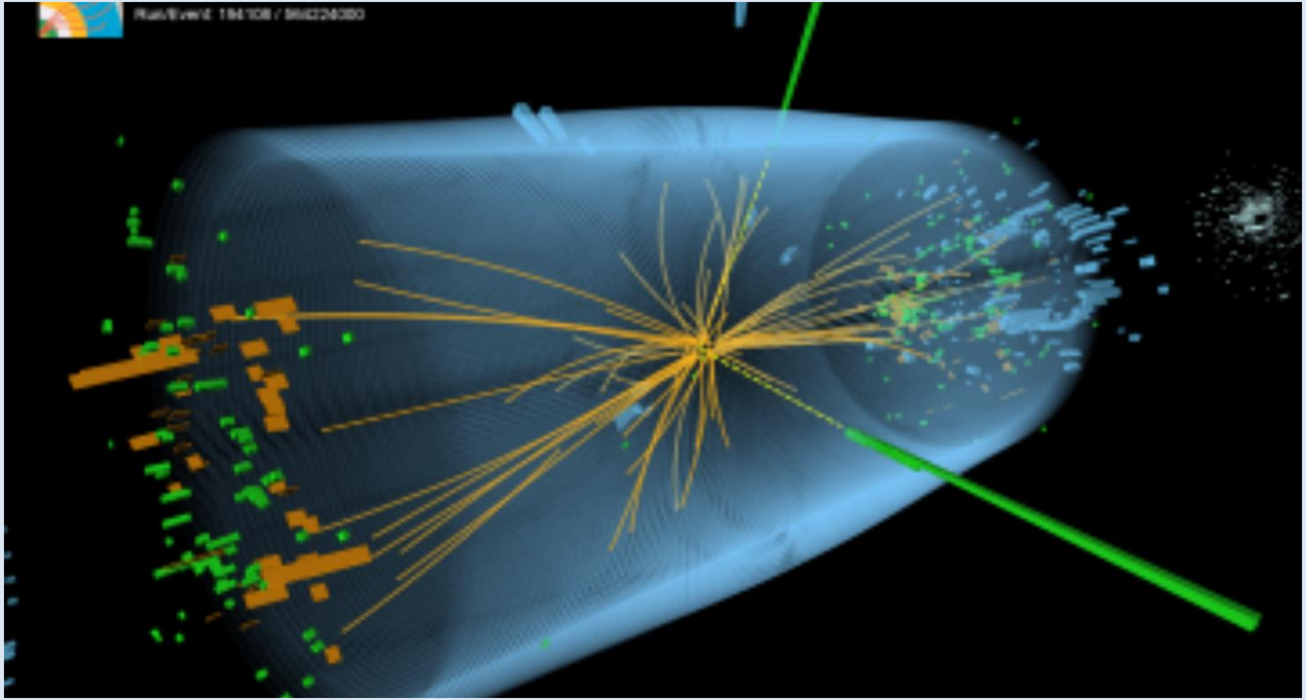

Process	Particle	Equipment
Shower shape in calorimeters	Electrons / Gammas	Calorimetry

e.m.

hadronic

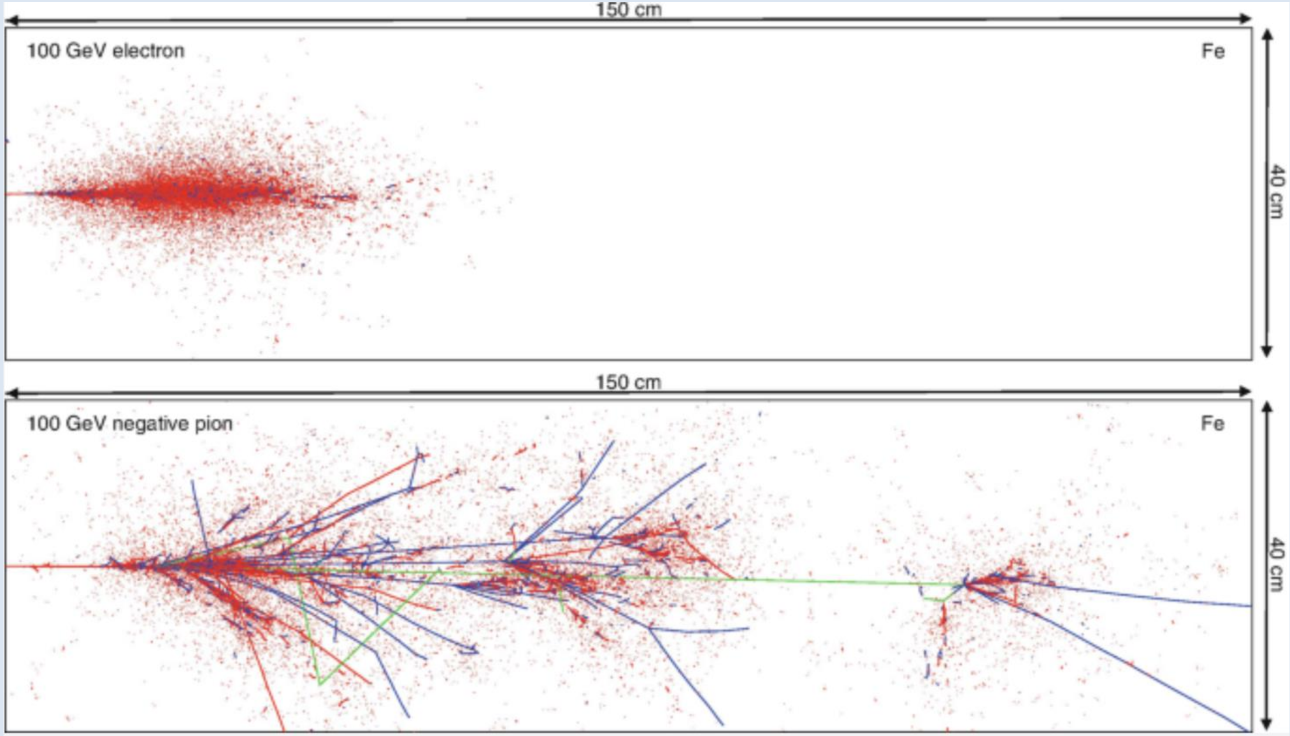

PID as Tracking By-product

Assume to know the momentum (by tracking the bending in a magnetic field)

$$p = \gamma\, m\, \beta c$$

Get the mass by measuring the velocity (βc)

Process	Particle	Equipment
Energy Loss (dE/dx)	Hadrons	Tracking
Transition Radiation (TDR)	Electrons	Tracking sensitive to X-ray
Time-of-Flight (TOF)	Hadrons	Timing
Cherenkov Radiation	Hadrons	Cherenkov

In tracking detectors we can measure the ionisation energy loss **d*E*/dx** by ionisation.

Bethe-Bloch equation:

$$-\frac{dE}{dx} = N_A \frac{2\pi\,\alpha^2(\hbar c)^2}{m_e c^2} z^2 \frac{Z}{A}\frac{1}{\beta^2}\left[\ln\left(\frac{2\gamma^2\beta^2 m_e c^2}{I_0}\right) - \beta^2 - \frac{\delta(\beta)}{2}\right]$$

Energy loss spectrum depends on βγ:

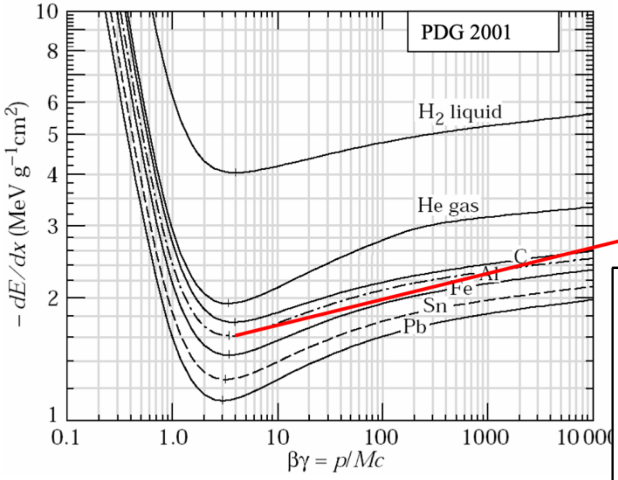

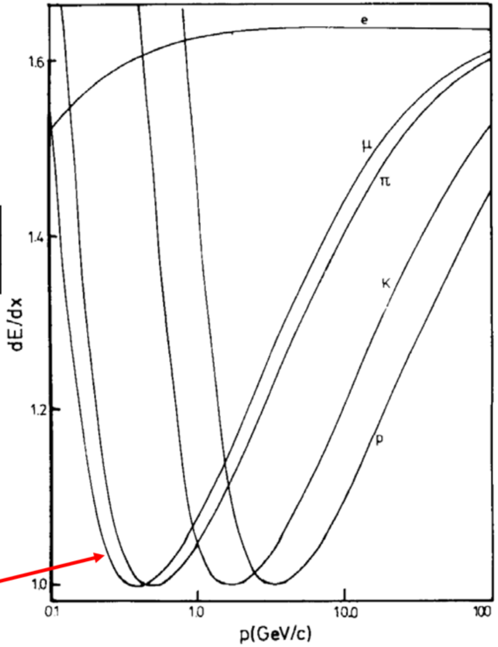

For different particle masses the spectra are shifted along ***p***.

Exception: Electrons have Bremsstrahlung.

Thus a simultaneous measurement of **d*E*/dx** and ***p*** provides information on the mass!

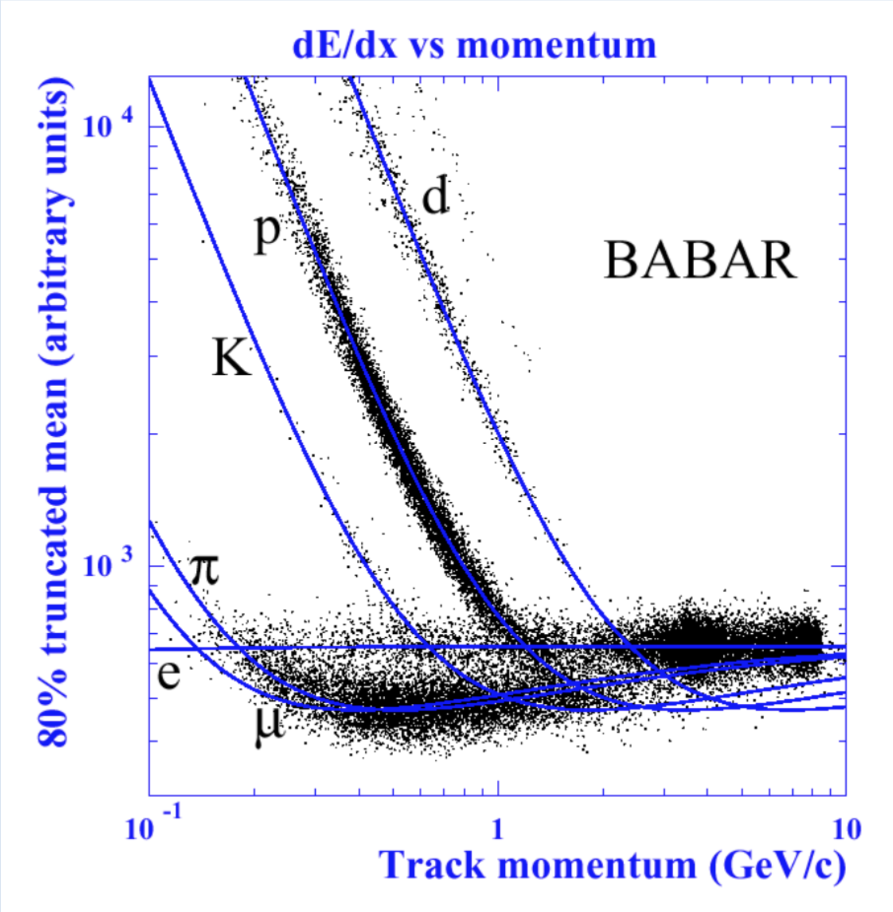

A by-product of a tracking detector

Average over several signals:
- many layers (straw tubes, silicon detctors)
- many electrodes over a big volume (TPC)

Different particles creates distinctive bands in the *dE/dx* vs *p* correlation plane

Identification is possible where the bands do not overlap (low energy)

A truncated mean is used to reject fluctuations

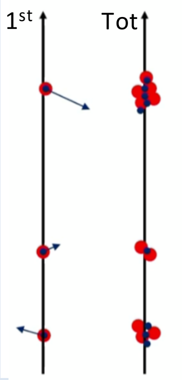

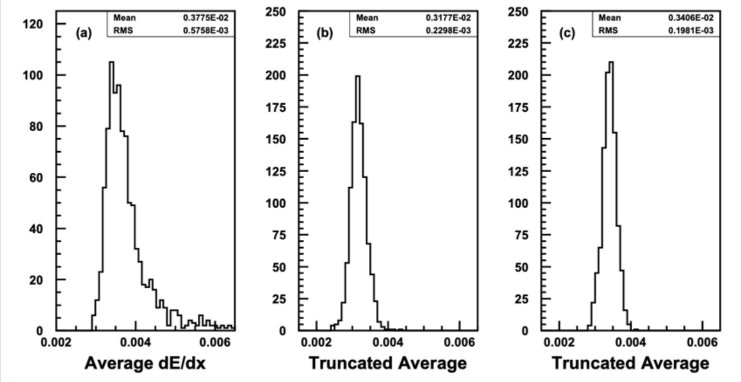

For thick layers or large sampling the dE distribution is approximated by a gaussian

For thin layers of small sampling rare hard-collisions matter (δ-rays, knock on electrons, bremmssthralung) and the dE distribution is described by a Landau distribution

$$\lambda = \frac{\Delta E - \Delta E_{mip}}{\epsilon}$$

$$P(\Delta E) = \frac{1}{\sqrt{2\pi}} e^{-\frac{1}{2}(\lambda + e^{-\lambda})}$$

A truncated mean is used to reject fluctuations or δ-rays and increase resolution

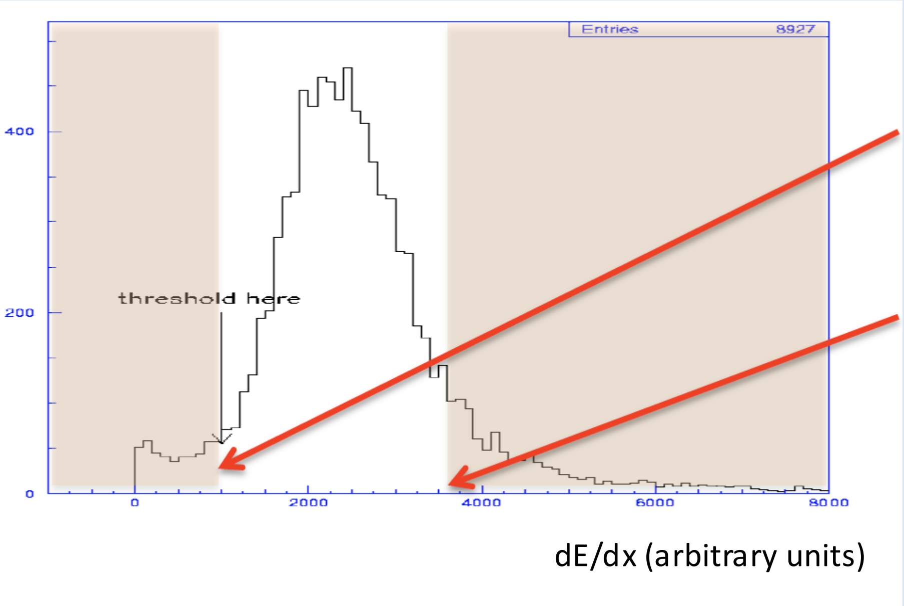

To remove background

To remove fluctuations

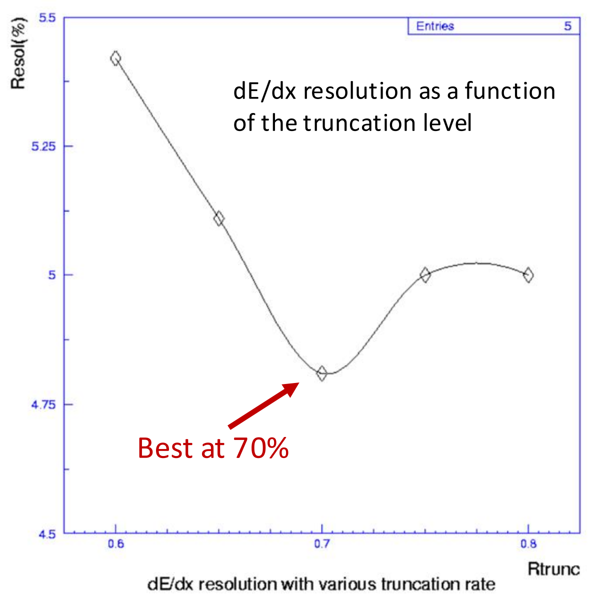

ALICE: Quark-gluon plasma in heavy ion collisions

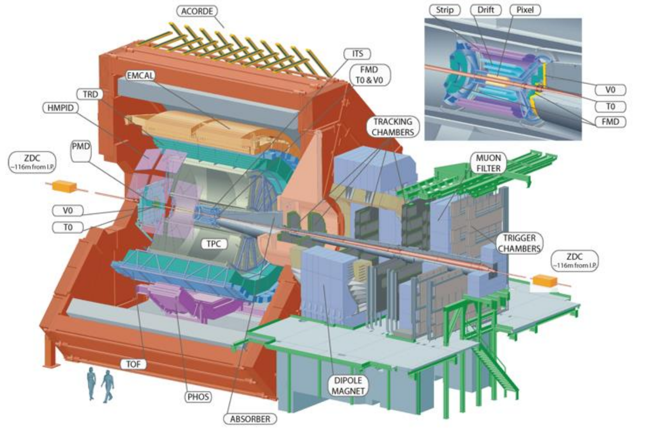

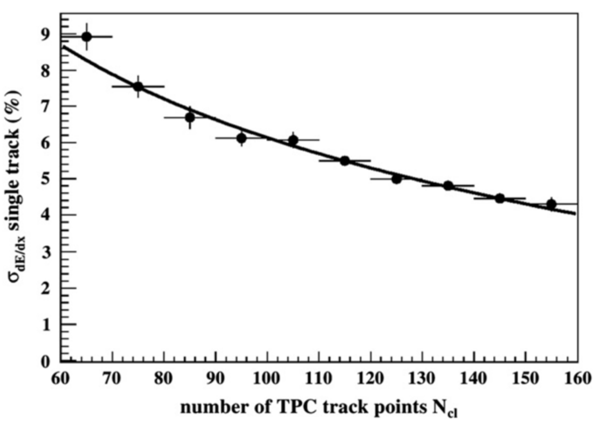

Time projection chamber

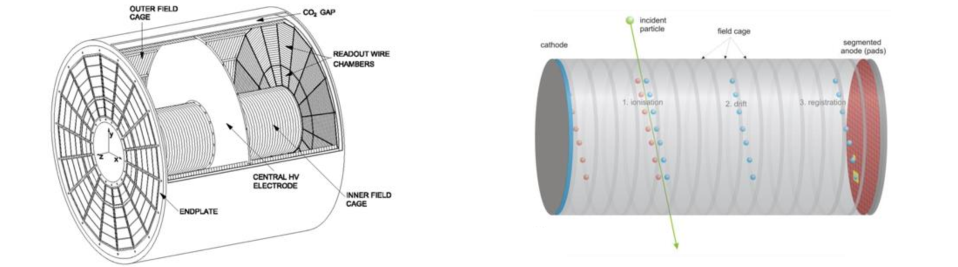

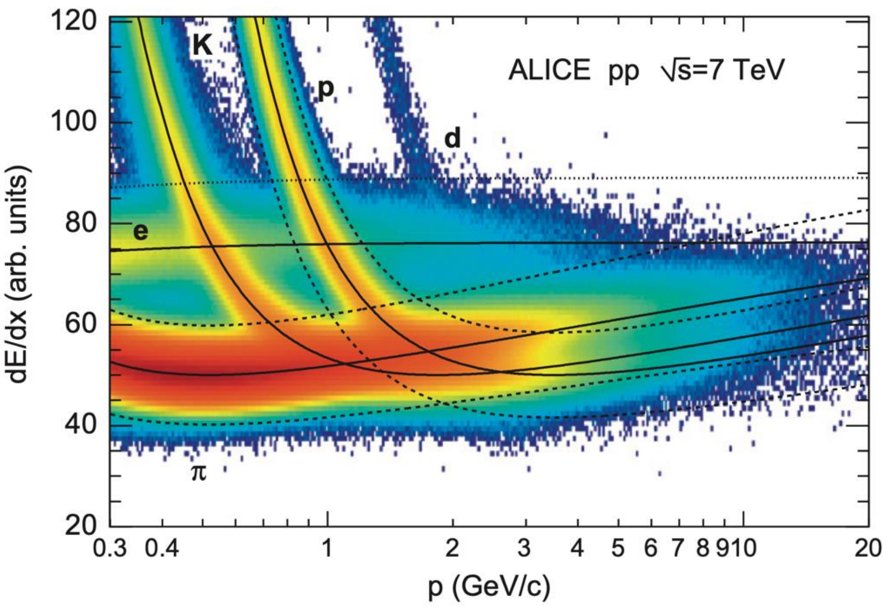

CMS: Higg boson and BSM search

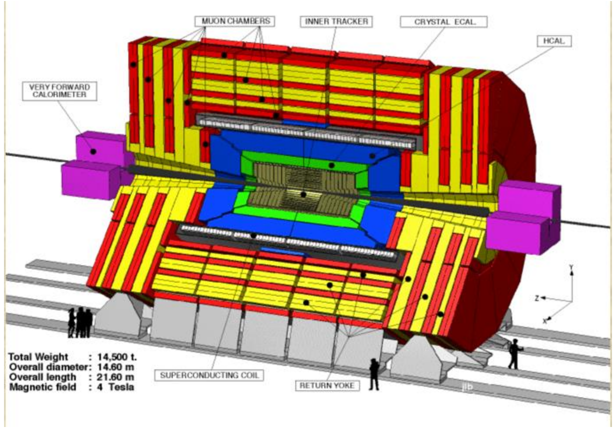

Momentum (GeV)	Resolution in (%)				
	Pixel	Silicon	Silicon+Pixel	MSGC	All Tracker
1.0	11.82	8.21	6.94	68.67	
2.0	11.08	8.03	6.64	35.08	
3.0	11.74	7.46	6.15	26.82	6.01
4.0	11.61	7.79	6.37	22.99	6.15
5.0	10.06	7.23	6.04	20.94	5.81
10.0	10.89	7.37	5.83	20.03	5.60

Inner Tracker System

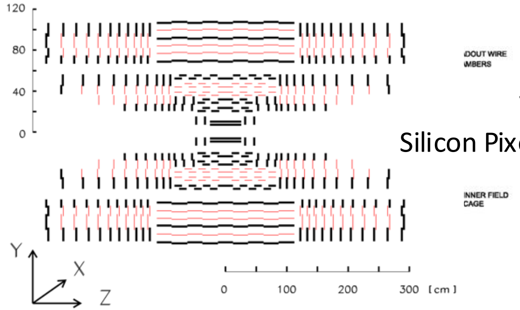

Micro-Strip Gas Chamber

Silicon Strip Detector

Silicon Pixel Detector

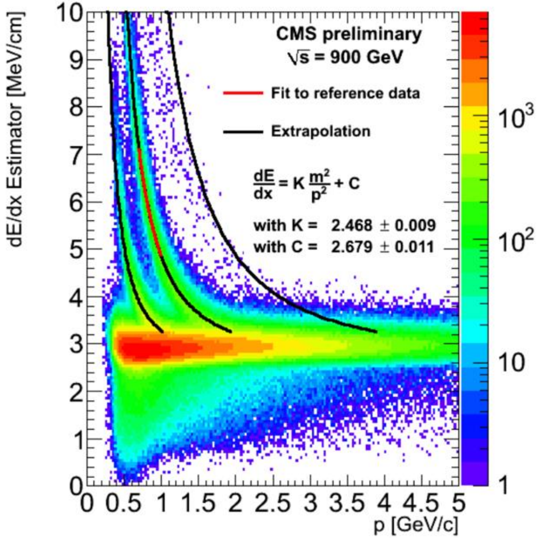

A particle passing the boundary between two media with different dielectric constants, will radiate photons. (predicted by Ginzburg & Frank 1946)

The energy radiated at one boundary: $E = \frac{1}{3}\alpha\,\gamma\,\hbar\omega_p$ $\left(\hbar\omega_p \approx 20\text{ eV for a plastic foil}\right)$

$\boldsymbol{E} \propto \gamma$: potential for electron identification at high momenta! (for electrons: $\gamma > 1000$)

The photon emission angle peaks at: $\theta \propto {}^{1}\!/_{\gamma}$ (very forward)

Typical photon energy: $E_\gamma \approx \frac{1}{4}\gamma\,\hbar\omega_p$

i.e. several keV for electrons. (detectable in proportional chamber with high Z gas!)

Photon yield per boundary is low: $\langle N_\gamma \rangle \approx \alpha \approx \frac{1}{137}$

Many transitions needed!

A typical design:

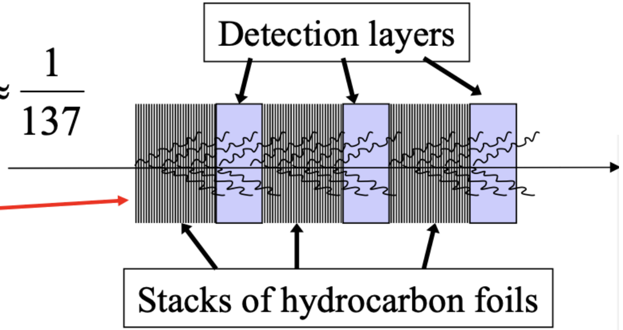

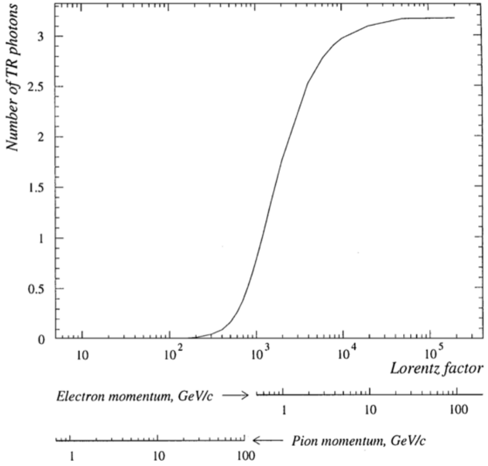

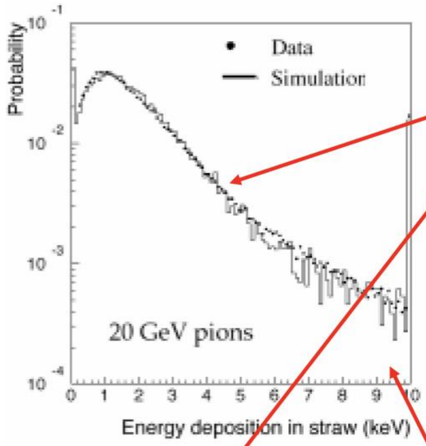

Energy deposited per layer

Pions: only ionisation energy loss (**d*E*/dx**)

Electrons: **d*E*/dx** plus transition radiation photons

<u>e/π separation:</u>

Count the number of hits with deposited energy greater than some threshold value: TR-hits

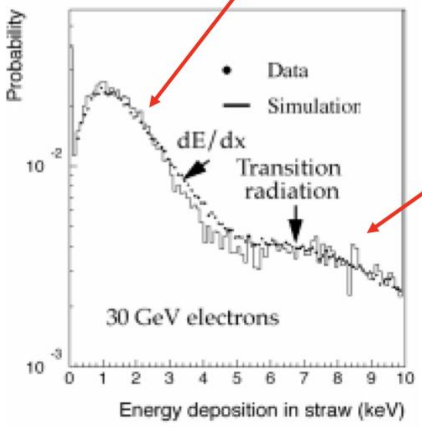

Good separation between $\pi^{\pm}$ and $e^{\pm}$.

Both at high and low momenta!

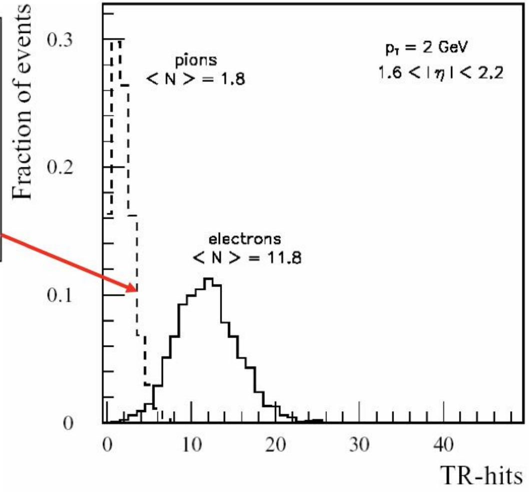

NOMAD: ν_u--> ν_e neutrino oscillations

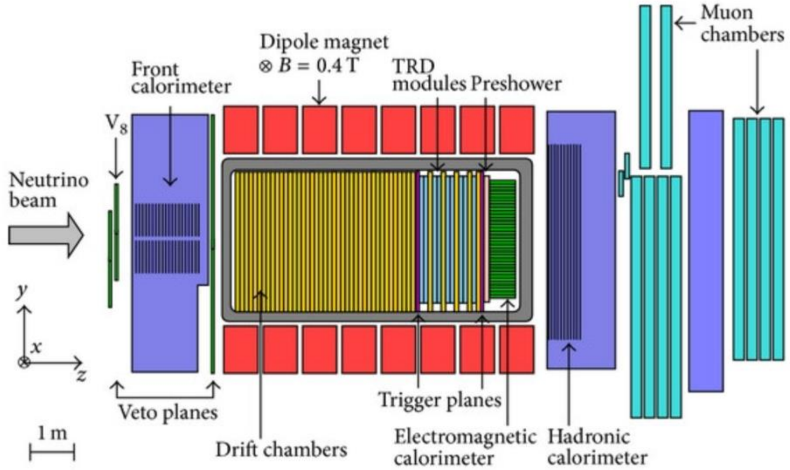

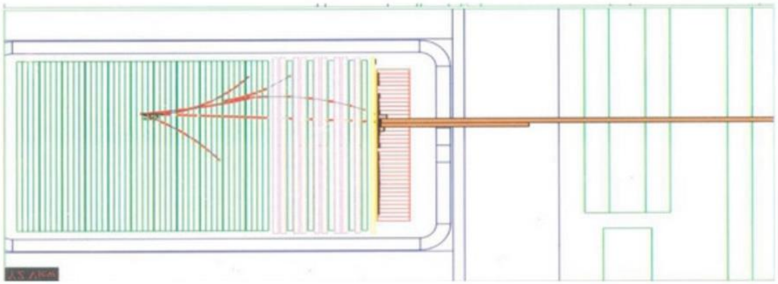

Transition Radiation Detector

315 x 15 μm polypropylene foils

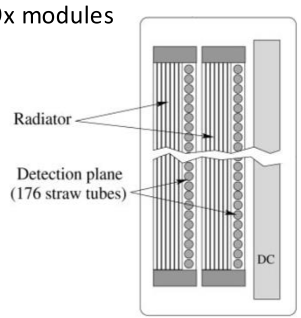

176 x 15 mm
Straw tubes
80% Xe + 20% CH_4

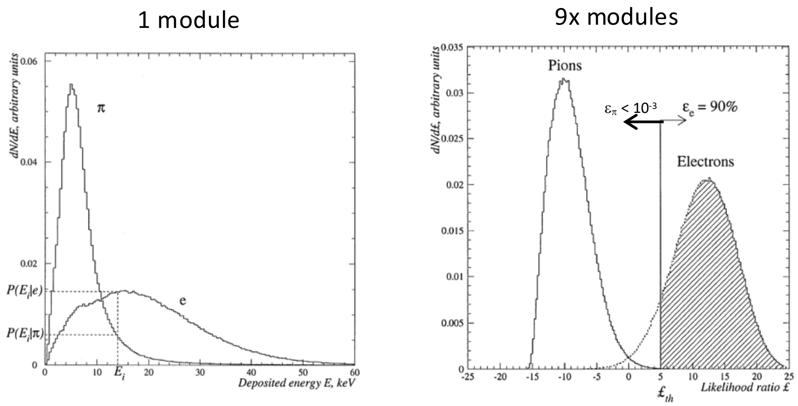

ATLAS: Higg boson and BSM search

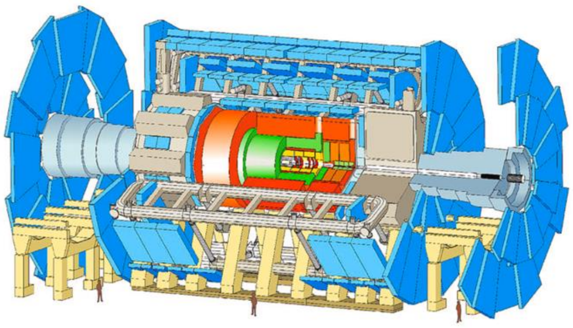

Tracking and transition radiation detector

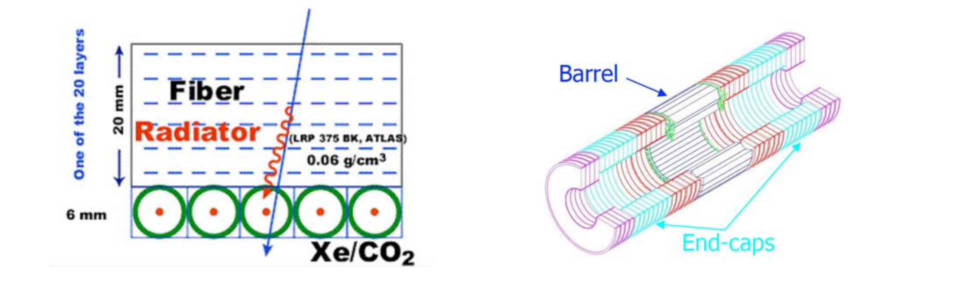

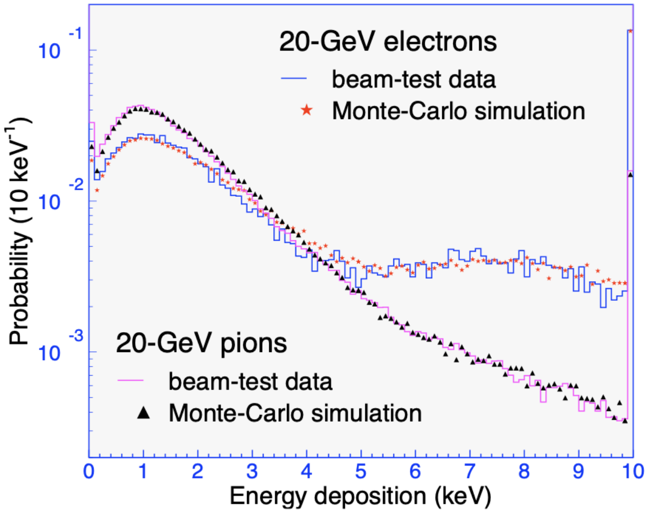

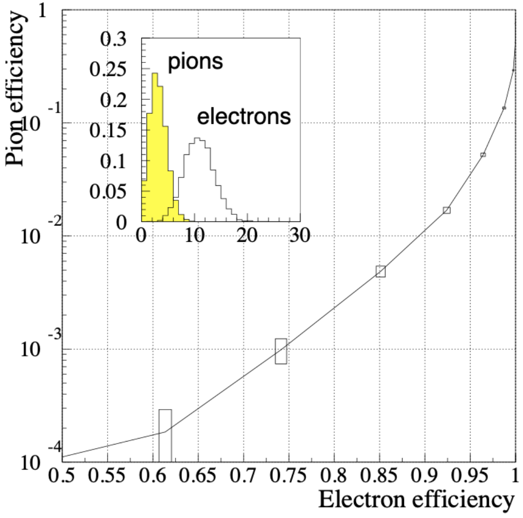

PID Sensors

Multi-Anode Photomultiplier (MA-PMT)

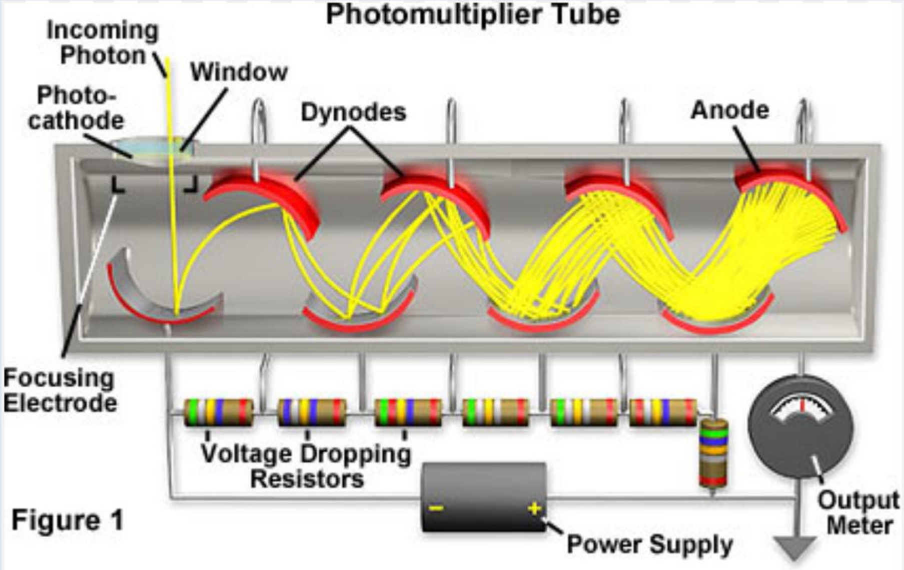

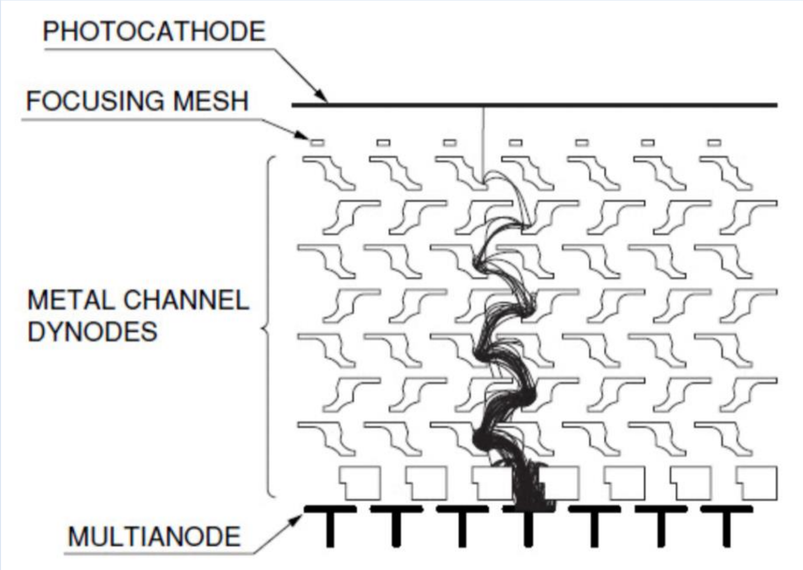

H8500 Flat Panel PMT

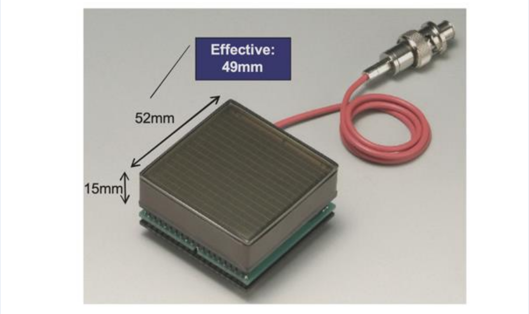

Pros.

- Compact Layout
- Cost-effective
- High packing-factor
- Position sensitive
- Fast, O(100 ps) TTS
- Low dark count

Cons.

- Complex Layout
- Magnetic Field Sensitive
- High-Voltage (~1 kV)

PMT Photocatode

Thin layer of alkali metal (mix) with very low work function in vacuum (to prevent contaminatino)

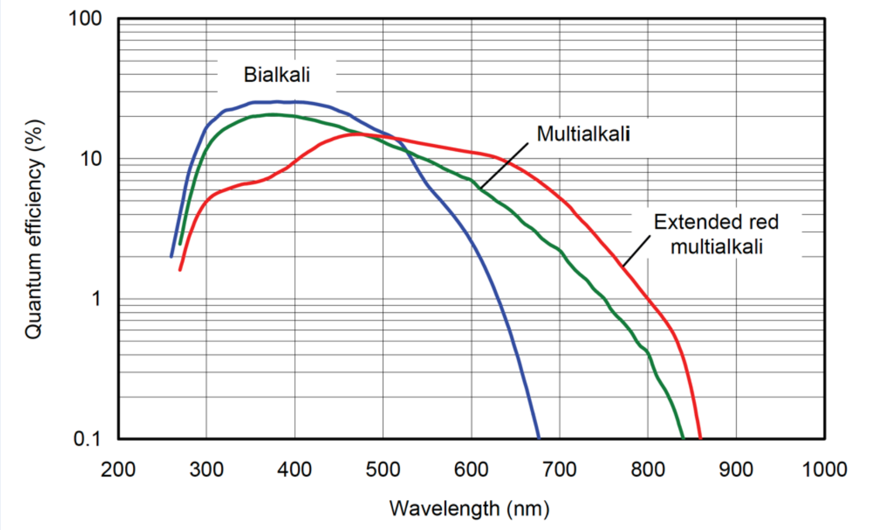

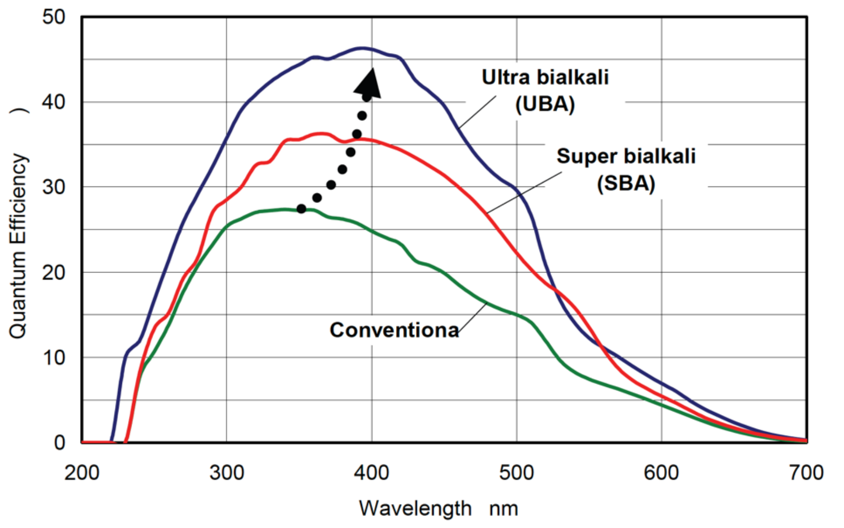

Photocatode optimization depends on the detail structure of PMTs

R7600
Compact
2x2 cm^2 area

Type No.	Spectral response: Range (nm)	Spectral response: Peak wavelength (nm)	Ⓐ Photo-cathode material	Ⓑ Window material	Ⓒ Dynode structure / stages	Maximum ratings: Supply voltage between anode and cathode (V)	Maximum ratings: Average anode output current in total (mA)	Cathode characteristics: Luminous Min. (μA/lm)	Cathode characteristics: Luminous Typ. (μA/lm)	Cathode characteristics: Blue sensitivity index (CS 5-58) Min.	Cathode characteristics: Blue sensitivity index (CS 5-58) Typ.	Cathode characteristics: Red/White ratio (R-68) Typ.	Cathode characteristics: Radiant Typ. (mA/W)
R7600U	300 to 650	420	BA	K	MC/10	900	0.1	60	80	7.5	9.5	—	80
R7600U-01	300 to 850	400	MA	K	MC/10	900	0.1	150	200	—	—	0.2	65
R7600U-03	185 to 650	420	BA	U	MC/10	900	0.1	60	80	7.5	9.5	—	80
R7600U-20	300 to 920	530	ERMA	K	MC/10	900	0.1	350	500	—	—	0.4	78
R7600U-100	300 to 650	400	SBA	K	MC/10	900	0.1	90	105	12.5	13.5	—	110
R7600U-200	300 to 650	400	UBA	K	MC/10	900	0.1	110	135	14.0	15.5	—	130
R7600U-300	300 to 700	420	EGBA	K	MC/10	900	0.1	120	160	12.0	14.0	—	125

NOTE: Ⓐ BA: Bialkali, MA: Multialkali, SBA: Super bialkali, UBA: Ultra bialkali, EGBA: Extended green bialkali, ERMA: Extended red multialkali

Micro-Channel Plate Photomultiplier (MCP-PMT)

Similarly of ordinary PMT – dynode structure is substitute by MCP

MCP: thin glass plate with an array of holes (10-100 μm diameter) continous dynode structure

Pros.

Gain 10^6 --> single photon

Collection efficiency 60%

Small thickness, High E field } Small transit time spread (~ 30 ps), Works in magnetic field

Segmented anode
--> Position sensitive

Cons. Expensive

(Ageing)

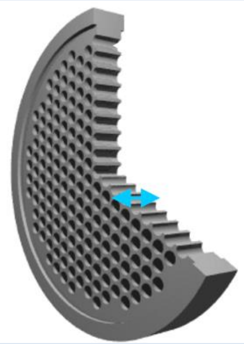

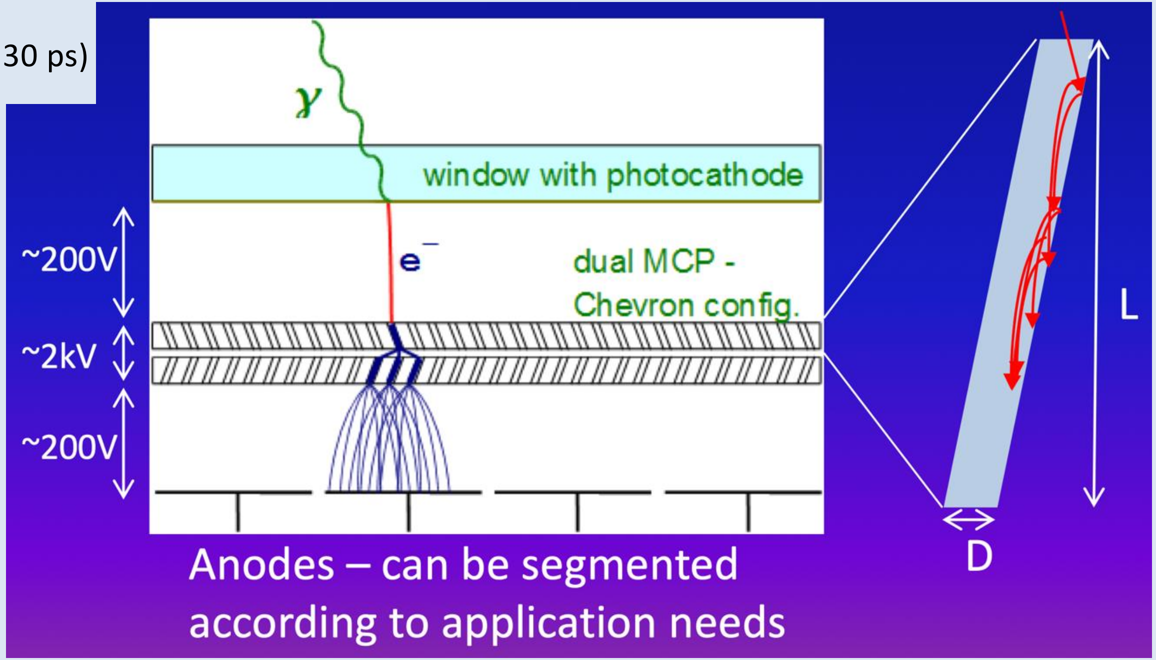

Micro-Channel Plate (MCP-PMT)

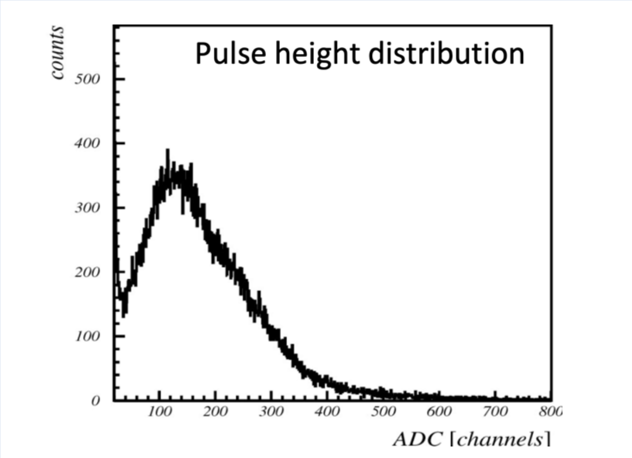

Gain is limited by space charge effects

Dynamic equilibrium --> gaussian pulse height distribution

Related to channel diameter

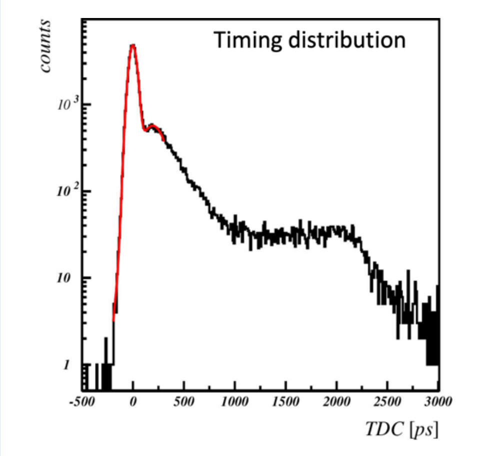

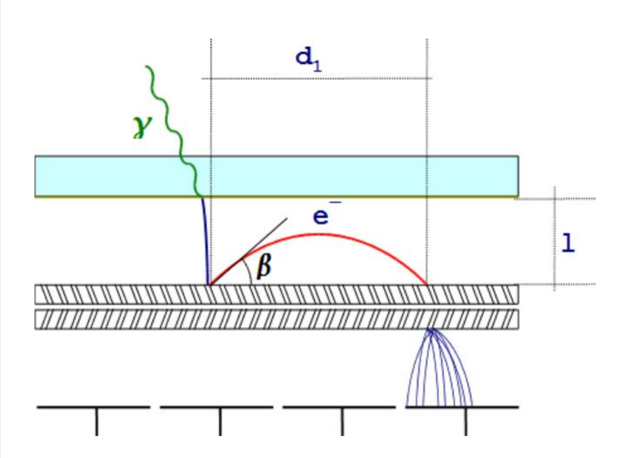

Photoelectron backscattering

Range equals twice the photocatode – MCP distance

long tail in time distribution and position resolution
Related to channel diameter

Narrow amplification channel sustains magnetic field (axial direction)

Backscattering reduced

Timing degraded

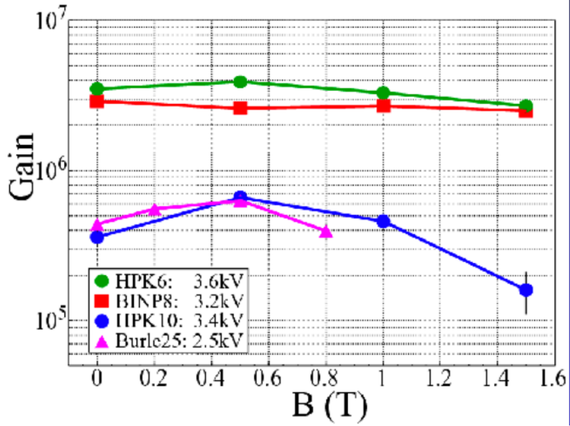

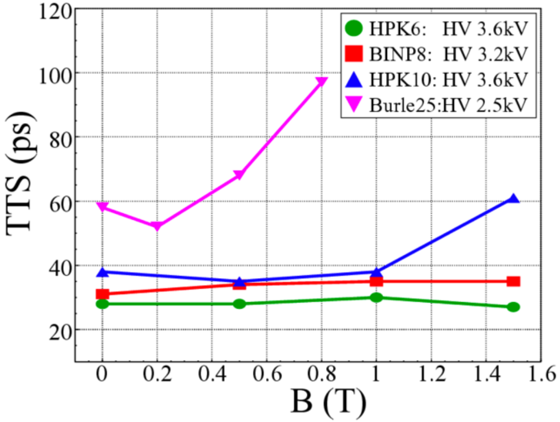

Residual gas ionization

QE degradation due to ion bombardment

Thin Al foil (few μm) block Ion feedback and ½ electrons

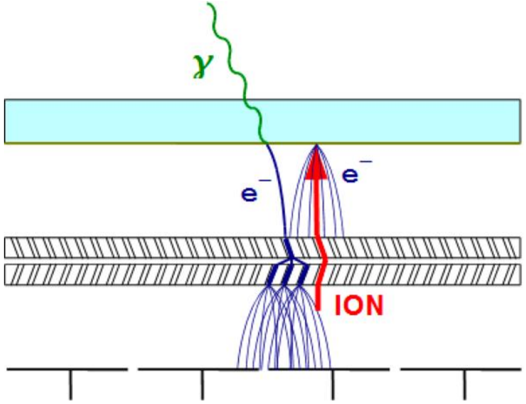

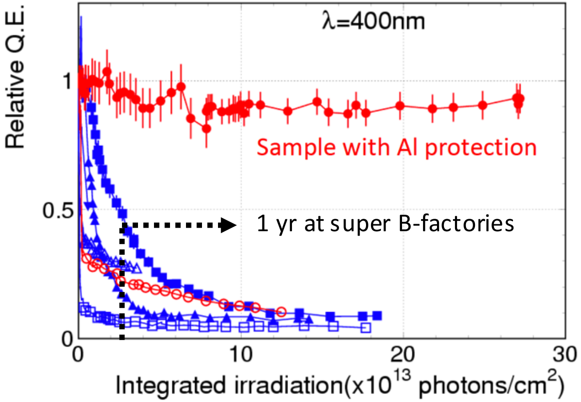

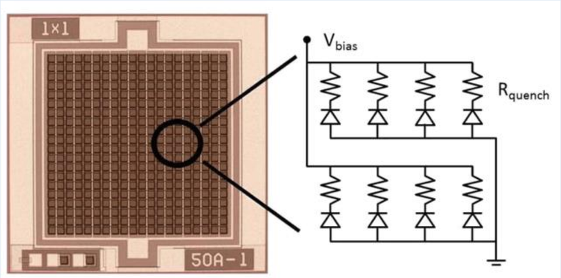

SPAD array on a common Si substrate

SPAD: single photon avalanche diode working in Geiger mode

R: quench resitor to stop the avalanche

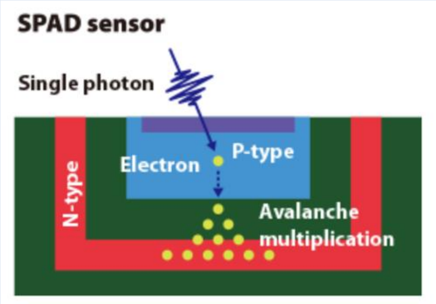

Fast rise (discharge) and slow recharge

Intrinsic high dark-count rate due to thermal electron (indistinguishable from single-photon)

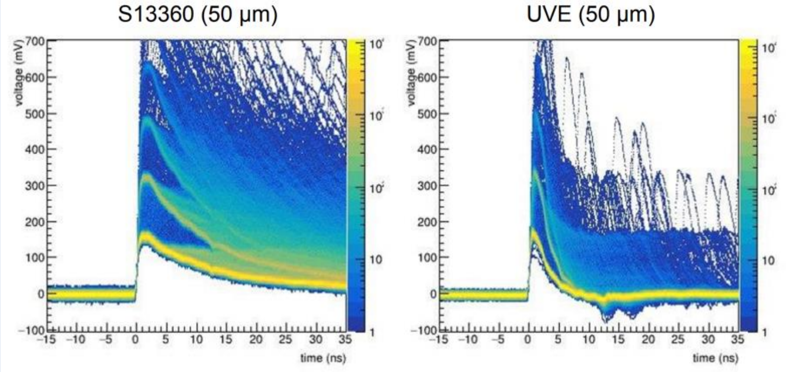

Possibility of

- single-photon detection
- photon counting

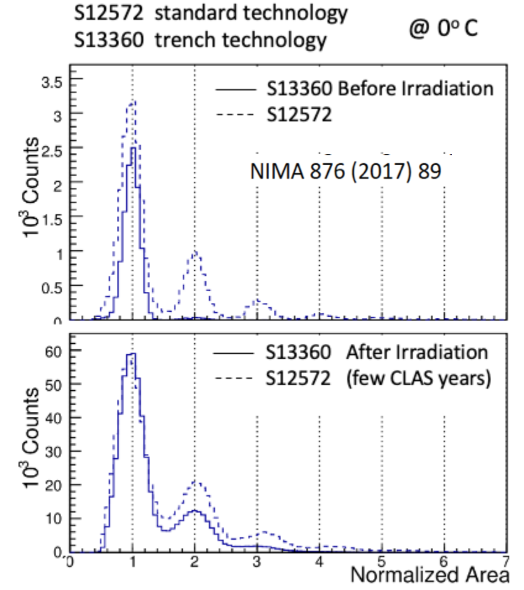

Silicon Photomultiplier (SiPM)

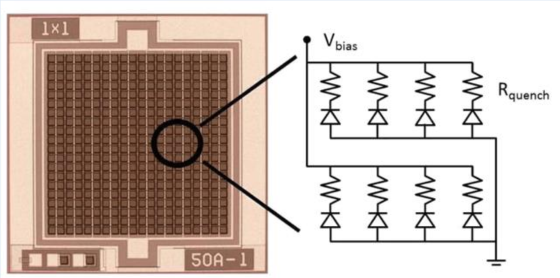

SPAD array on a common Si substrate

SPAD: single photon avalanche diode working in Geiger mode

R: quench resitor to stop the avalanche

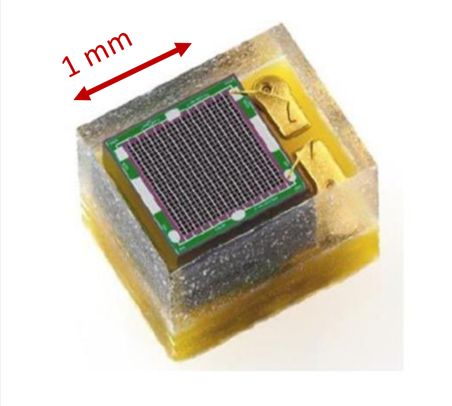

5 cm

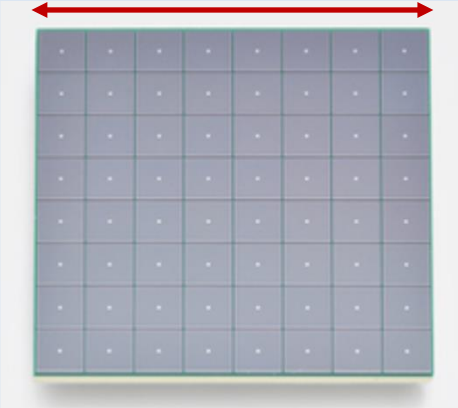

- **pros**

Compact & robust layout

Cost-effective production process

High photon efficiency (40-50%)

Good time resolution (~ 100 ps)

Insensitive to magneti field (used for NMR)

- **cons**

High dark count rates

Radiation sensitive

→ Cooling
Timing
Annealing

Dark counts can be mitigated by working at low temperature (about 0.5x every 10 degrees)
Radiation damage can be cured with high-temperature annealing cycles

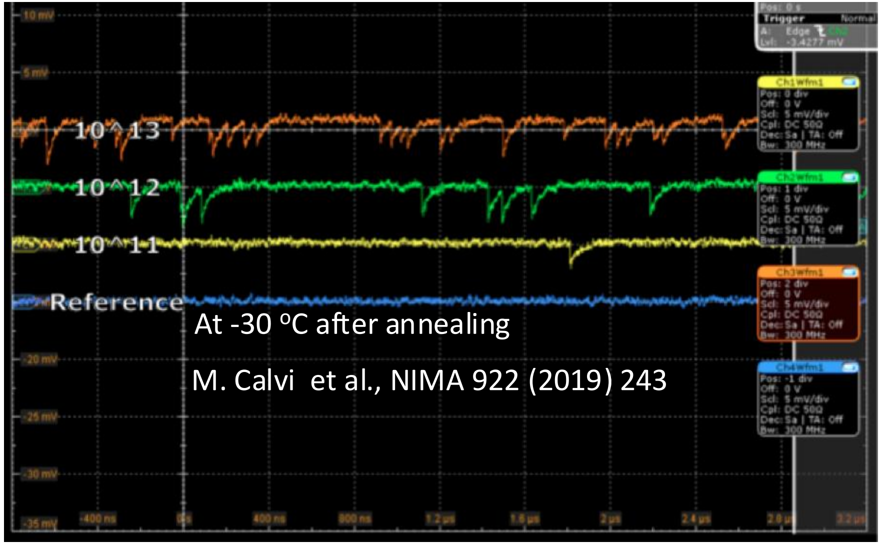

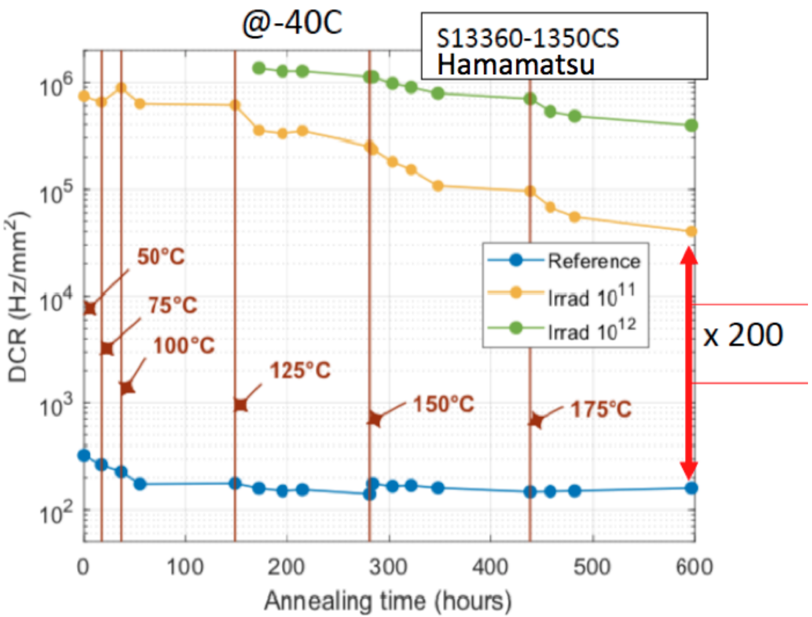

Specific PID Detectors

Use momentum (tracking) to get the mass $p = \gamma\, m\, \beta c$

Process	Particle	Equipment
Energy Loss (dE/dx)	Hadrons	Tracking
Transition Radiation (TDR)	Electrons	Tracking sensitive to X-ray
Time-of-Flight (TOF)	Hadrons	Timing
Cherenkov Radiation	Hadrons	Cherenkov

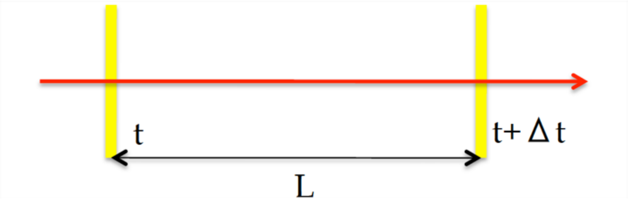

$$\frac{L}{\Delta t} = \beta c = \frac{pc^2}{E} = c^2 \frac{p}{\sqrt{p^2c^2 + m^2c^4}} = c\frac{p}{\sqrt{p^2 + m^2c^2}}$$

$$\frac{\Delta t}{L} = \frac{1}{c}\sqrt{\frac{p^2 + m^2c^2}{p^2}} = \frac{1}{c}\sqrt{1 + \frac{m^2c^2}{p^2}}$$

if $\frac{m^2c^2}{p^2} << 1$ then $\sqrt{1 + \frac{m^2c^2}{p^2}} \approx 1 + \frac{m^2c^2}{2p^2}$

$$\Delta t_1 - \Delta t_2 = \frac{Lc}{2p^2}\left(m_1^2 - m_2^2\right)$$

Δt = TOF

L = flight distance

Start time t and distance L should be known*

Arrival time difference goes with m^2

drops as p^2

* With negligible uncertainty

Time-of-flight

$$n\,\sigma = \frac{\Delta t_1 - \Delta t_2}{\sigma} = \frac{L}{2c\sigma}\frac{(m_1^2 - m_2^2)}{p^2}$$

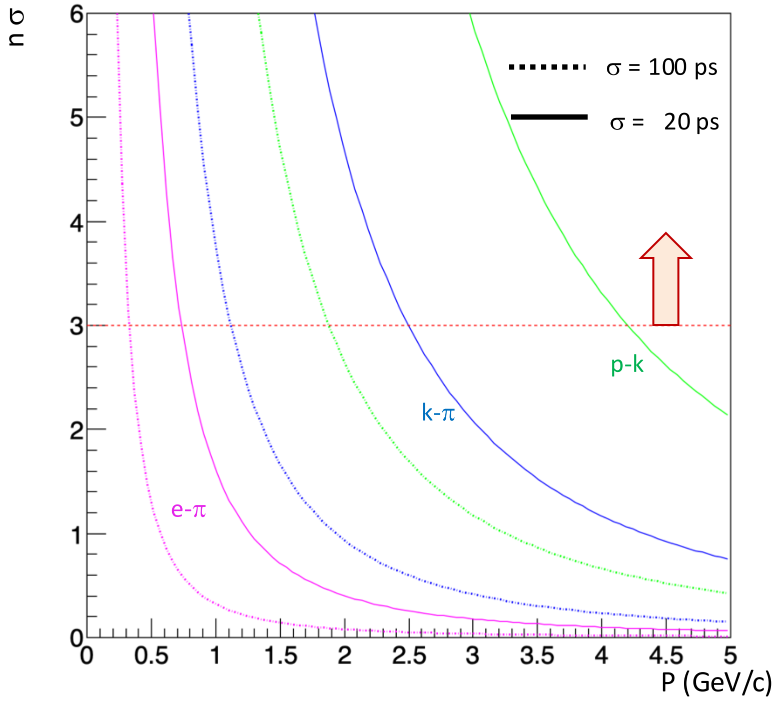

c ~ 10^8 m/s = 0.3 m/ns = 0.03 m / 100 ps

Reference requirement is a at least 3σ separation

To double the reach in momentum one needs to quadruplicate distance or time precision

With typical values

leverage *L* of 1 m

time resolution σ ≲ 100 ps

raw limits are

e-π ≲ 1 GeV/c
k-π ≲ 3 GeV/c
p-k ≲ 5 GeV/c

CLAS12: Nucleon structure and spectroscopy

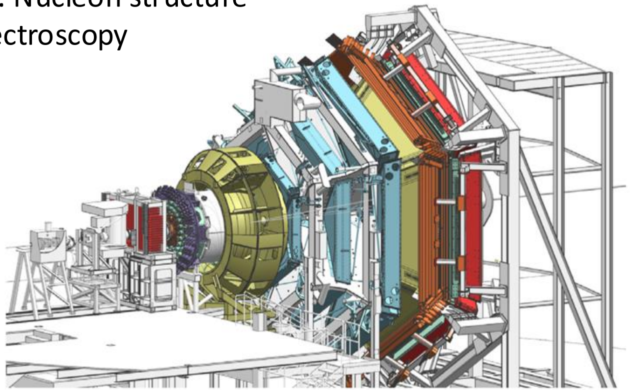

Scintillator bar + PMT

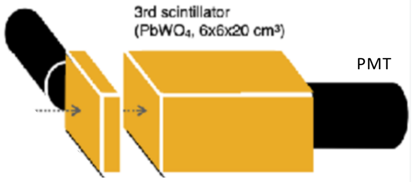

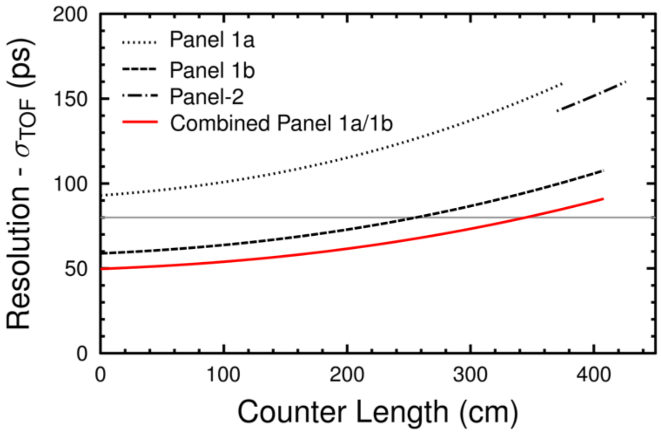

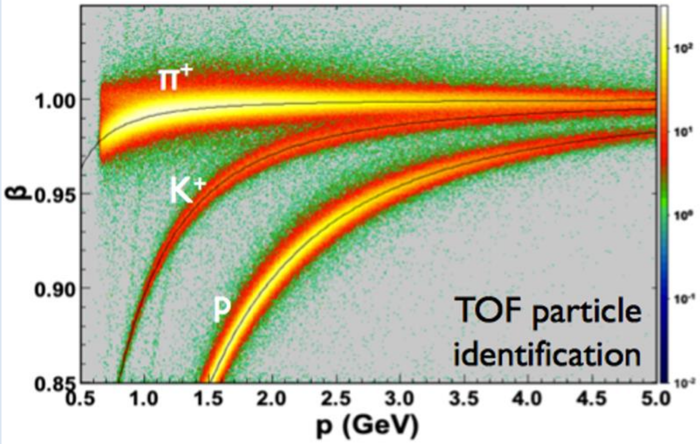

$$\sigma_{TOF} = \sqrt{\sigma_0^2 + \frac{\sigma_1^2 + (\sigma_2 L/2)^2}{N_{pe}}}$$

σ_0 intrinsic electronics resolution of the readout chain, independent of light level

σ_1 time jitter in the combined single-photon response of the scintillation counter and PMT

σ_2 path length variations in the light collection, that scales with distance from source

$$N_{pe} = N_{pe}^0 \exp\left(\frac{L_0}{2\lambda_0} - \frac{L}{2\lambda}\right) \cdot F$$

For large bars, the variations in path length are the dominant contribution to the resolution

λ_0 reference attenuation length

L_0 length of the shorter bar

F PMT collection efficiency (active fractional area)

M. Bohm et al., JINST 11 (2016) C05018 – PANDA TOF

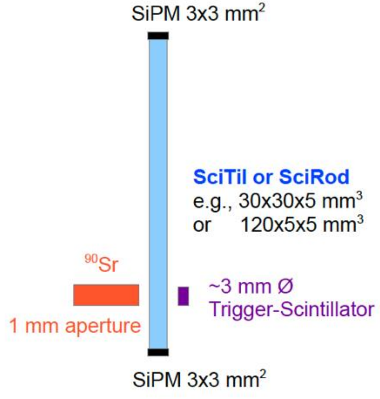

(a) schematic

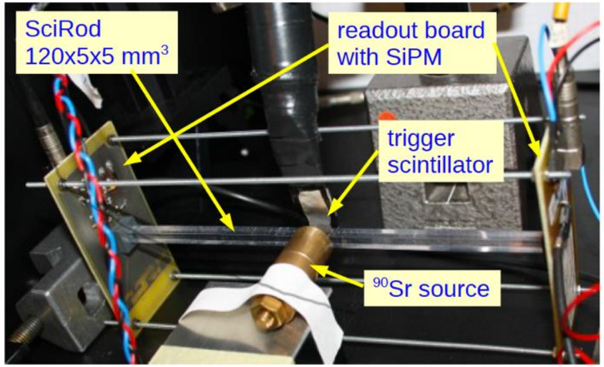

(b) photograph

scintillator size	MPPC	BC408	BC420
$170 \times 5 \times 5\,\text{mm}^3$	S10362-050P	97 ± 19	
$120 \times 5 \times 5\,\text{mm}^3$	S12652-050C	81 ± 12	68 ± 10
$50 \times 5 \times 5\,\text{mm}^3$		83 ± 6	62 ± 5
$120 \times 10 \times 5\,\text{mm}^3$	S10362-100P	105 ± 18	93 ± 25
$50 \times 10 \times 5\,\text{mm}^3$	S12572-050P	109 ± 16	

T. Rostomyan, Nucl. Instrum. Meth. A 986 (2021) 164801 – MUSE experiment

Table A.2: Time resolutions and efficiencies for 3 mm thick, 300 mm long and 12 mm wide BC-404 BM paddles. All results are better than the experimental requirements.

Scintillator	SiPM	σ_T (ps)	ϵ (%)
BC-404	S13360-3075PE	59	≥ 99.9
BC-404	S13360-3050PE	60	≥ 99.7
BC-404	ASD-NUV3S-P-40	65	≥ 99.0

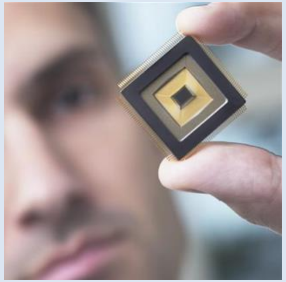

Option to cover the rod rims with SiPMs connected in series (full coverage with 1 readout channel)

ALICE: Quark-gluon plasma in heavy ion collisions

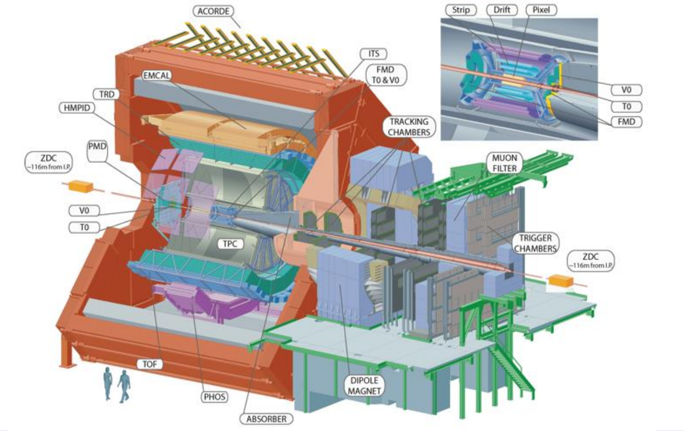

Multigap resistive plate chamber

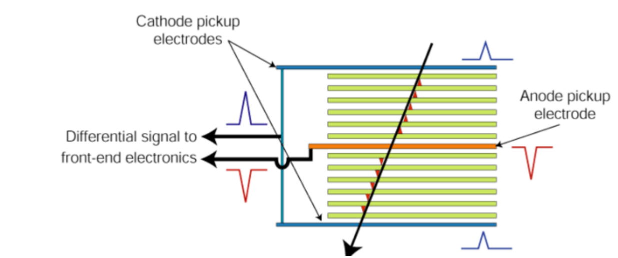

Fem mm gas gaps with local streamer discharge (position sensitive)

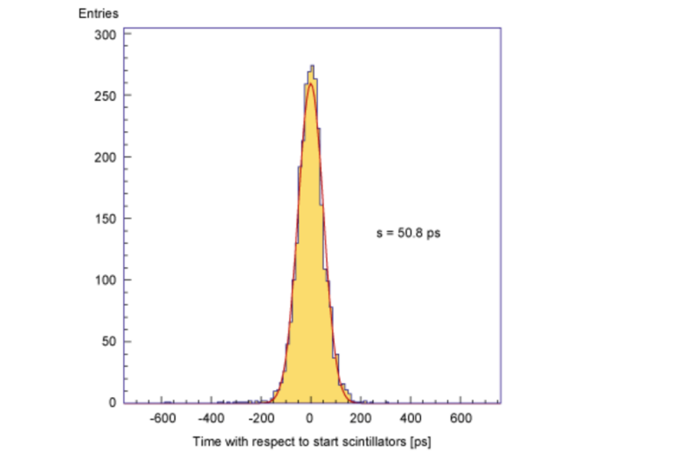

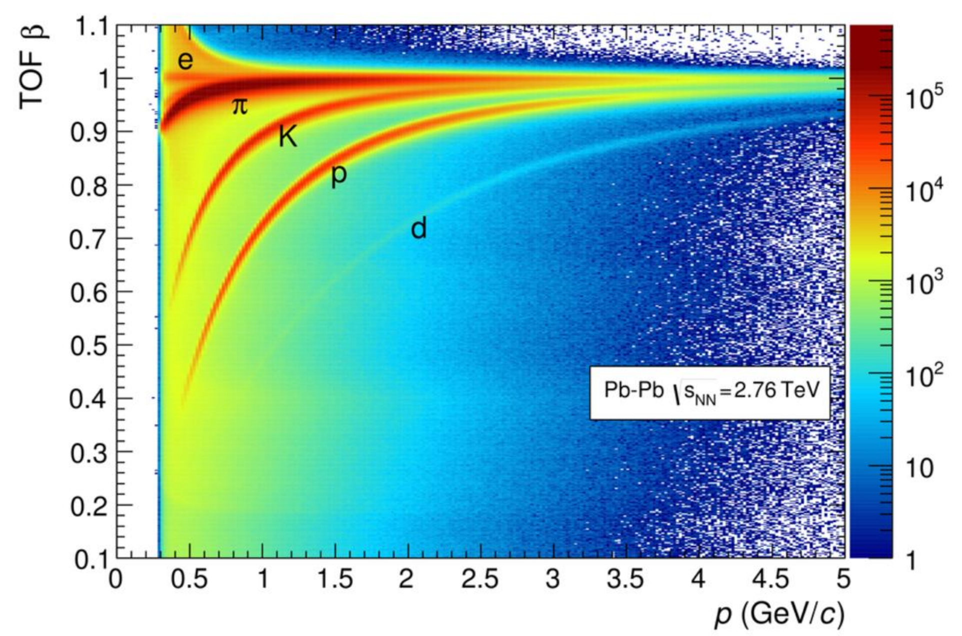

Photo emission by a charged particle travelling in a dielectric medium with a velocity greater than the velocity of light in that medium:

$$\cos\theta_c = \frac{(c/n)\Delta t}{\beta c \Delta t} = \frac{1}{\beta n} \qquad v_{\text{particle}} > \frac{c}{n} \quad \left(\beta_{\text{thr}} = \frac{1}{n}\right)$$

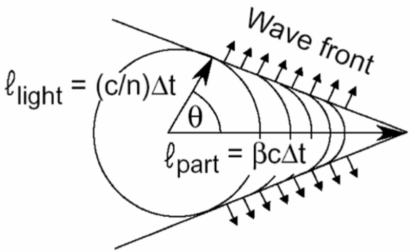

Momentum threshold:

$$\epsilon = n - 1$$

$$\beta = \frac{p}{\sqrt{p^2+m^2}} = \frac{1}{1+\epsilon} \quad \Rightarrow \quad p = \frac{1}{\sqrt{2\epsilon+\epsilon^2}} \cdot m$$

Scales with particle mass

Decreases with n

Photon yield:

$$\frac{d^2N}{d\lambda dx} = \frac{2\pi z^2\alpha}{\lambda^2}\left(1 - \frac{1}{\beta^2 n^2(\lambda)}\right)$$

$$\frac{dN}{dx} = 2\pi z^2 \alpha \sin^2\theta_C \left(\frac{1}{\lambda_1} - \frac{1}{\lambda_2}\right)$$

$\propto$ **$\sin^2(\theta_c) = 1-(1/\beta n)^2 \Rightarrow$ small when $n \approx 1$!**

$\propto$ **$1/\lambda^2 \Rightarrow$ mostly blue light!**

$$\hbar c = 2 \cdot 10^{-5} \ \text{eVcm}$$

$$\frac{d^2N_{ph}}{dLdE}[\text{cm}^{-1}\text{eV}^{-1}] = \frac{\alpha Z^2}{\hbar c}\sin^2\theta = 370 Z^2 \sin^2\theta \qquad E_{ph}[\text{eV}] = 2\pi\hbar\frac{c}{\lambda} = \frac{1240}{\lambda[\text{nm}]}$$

Exp.	Mezzo	n	θ (^{o})	$N_{ph} = 370 \cdot \sin^2\theta$ ($eV^{-1}cm^{-1}$)	p_π in soglia (GeV)
	Helio	1.000035	0.48	0.026	16.1
	Air	1.000283	1.36	0.208	5.6
	Argon	1.000282	2.66	0.796	3.003
E835	CO_2	1.000410	1.64	0.302	4.873
	CH_4	1.000436			
LHCb/EIC	CF_4	1.0005	1.81	0.370	4.396
E835	Freon 13	1.000720	2.17	0.530	3.677
EIC	C_2F_6	1.00082	2.32	0.606	3.432
E835	Freon 12	1.001080	2.66	0.796	3.003
	Isobutano	1.00147	2.89	0.941	2.67
Hermes/LHCb	C_4F_{10}	1.0014	3.03	1.033	2.55
Hermes	Aerogel	1.03 (1.015-1.08)	13.9	21.23	0.55
	Freon	1.233	35.8	126.6	0.19
	Aqua	1.33	41.2	160.8	0.15
	Quarzo	1.46	46.7	196.4	0.126
	BGO	2.15	62.3	290	0.070

1 m (Helio – C_4F_{10})

few cm (Aerogel)

Real PID starts at 3x (kaon)

Photon Detection

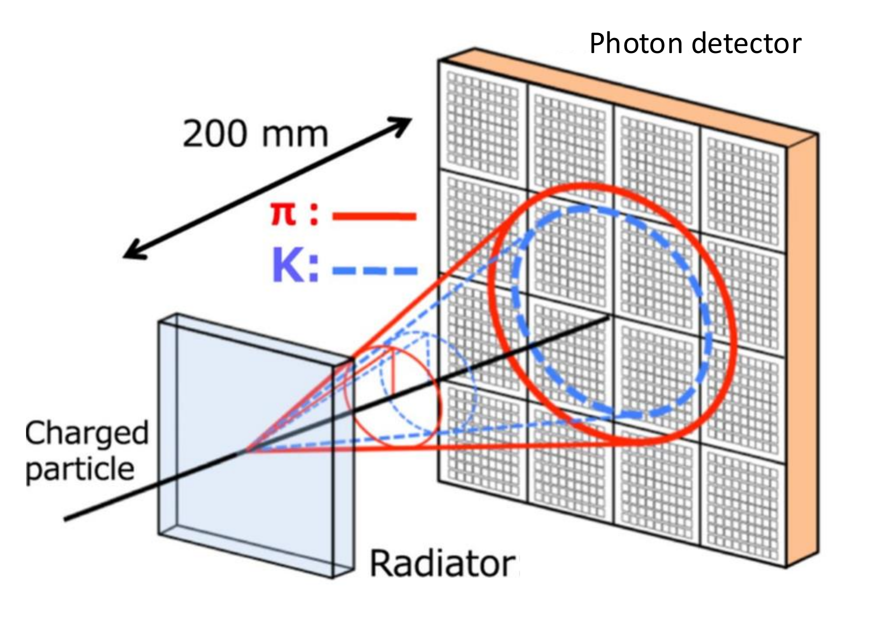

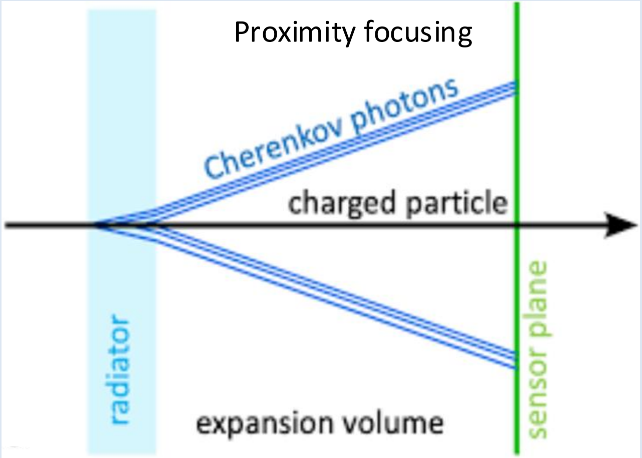

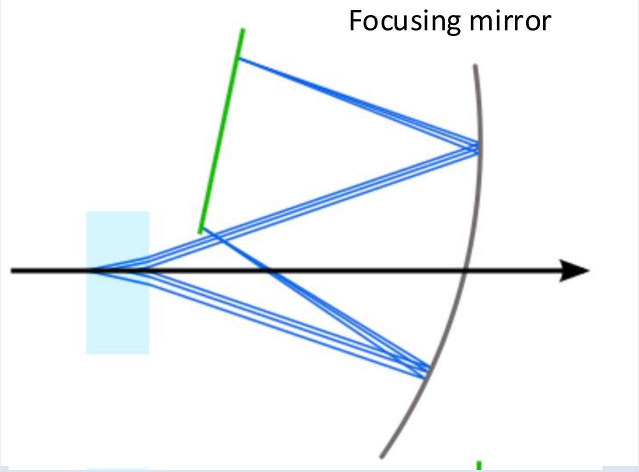

Photon Yield

Spectrum of Cherenkov photons

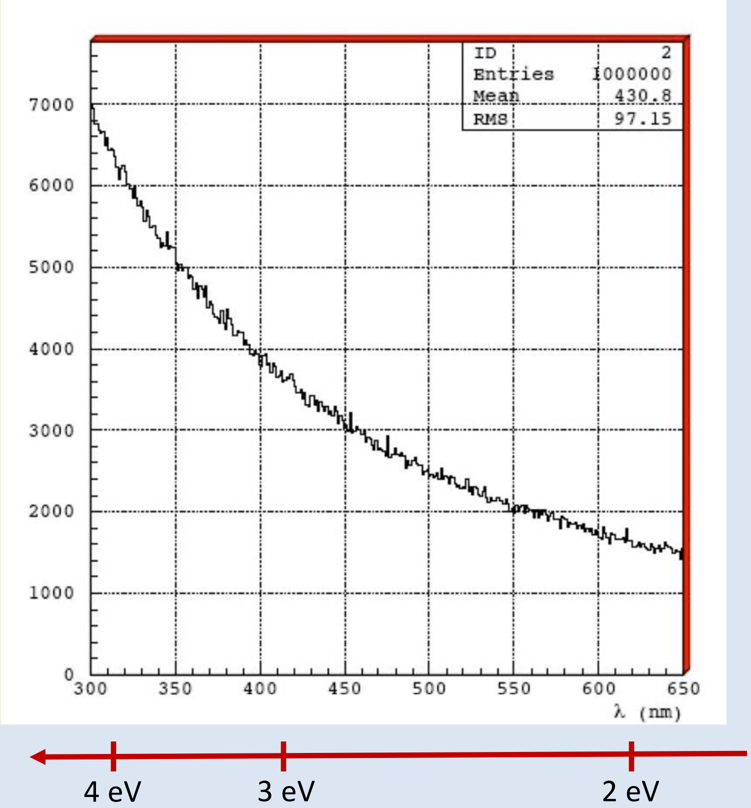

Typical sensitivity (quantum efficiency) of a PMT

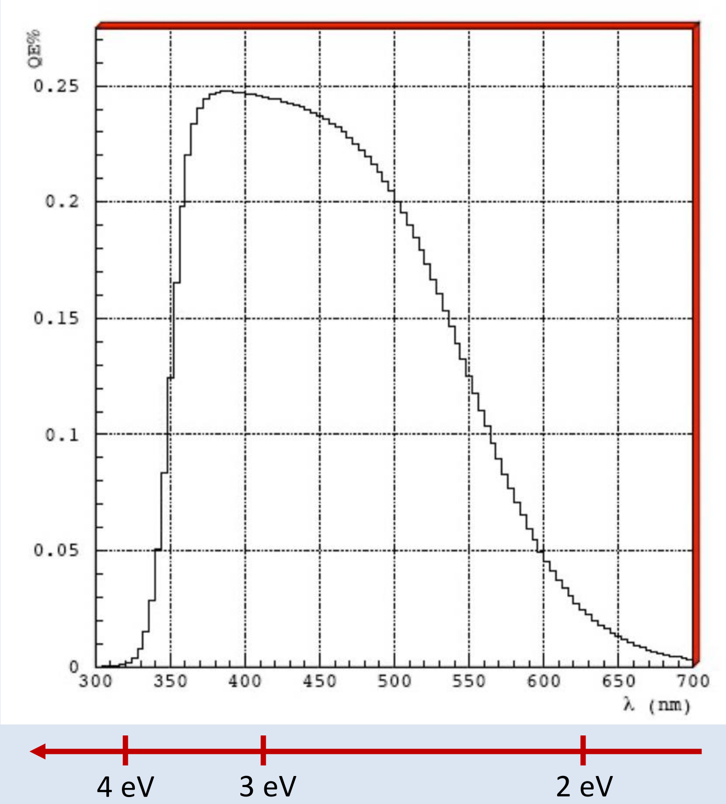

Gas Radiator

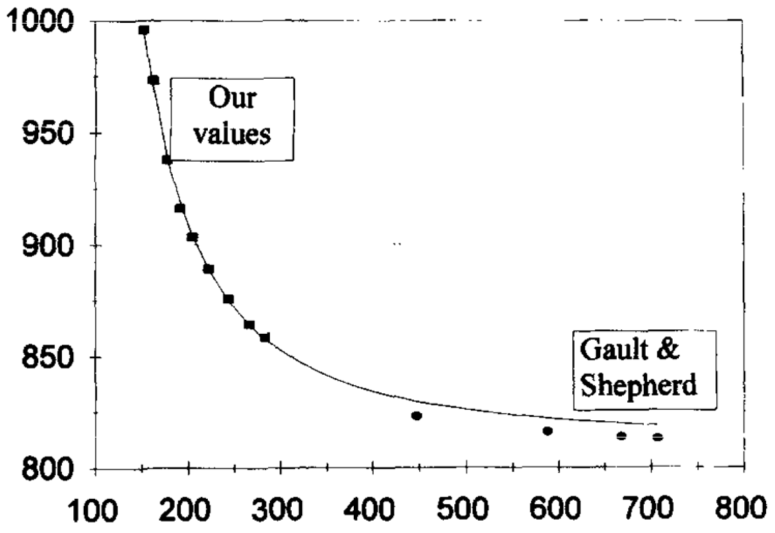

Fig. 1. The refractivity of C_2F_6 (hexafluoroethane) expressed as $(n-1)\times10^6$ is plotted versus the wavelength in nm. The solid line corresponds to the Sellmeier formula fitted with our measurements.

Aerogel Radiator

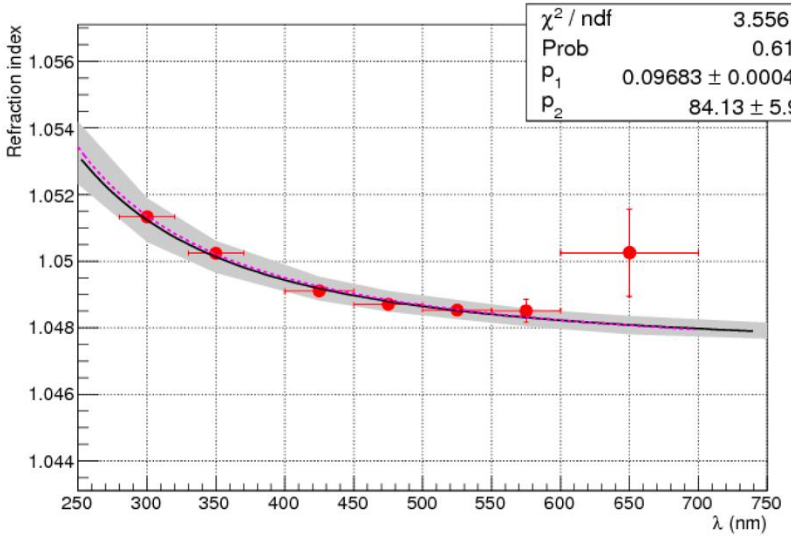

Refractive index as a function of the Cherenkov light wavelength for the aerogel with n = 1.05 and trad = 20 mm obtained selecting pions with 8 GeV/c momentum.

Sellmeier parameterization $$n^2(\lambda) = 1 + \frac{p_1\lambda^2}{\lambda^2 - p_2^2}$$

$$\sigma_{CH} = \sqrt{\sigma_{Co}^2 + \frac{\sigma_{em}^2 + \sigma_{ch}^2 + \sigma_{px}^2}{N_{pe}}}$$

σ_{co} correlated uncertainty (tracking, misalignment, magnetic bending, multiple scattering, ….)

σ_{em} uncertainty on the photon emission point (radiator depth)

σ_{ch} radiator chromatic dispersion

σ_{px} sensor spatial resolution (pixel size)

$$\frac{d^2N}{dxd\lambda} = \left(\frac{d^2N_C}{dxd\lambda}\right) QE(\lambda)\epsilon_{pe} e^{-\frac{t_{rad}-x}{\Lambda(\lambda)\cos(\eta_C)}}$$

$Q(\lambda)$ Sensor quantum efficiency

$\Lambda(\lambda)$ Radiator transmission length

ε_{pe} detection efficiency (sensor and mirror)

t_{rad} radiator thickness

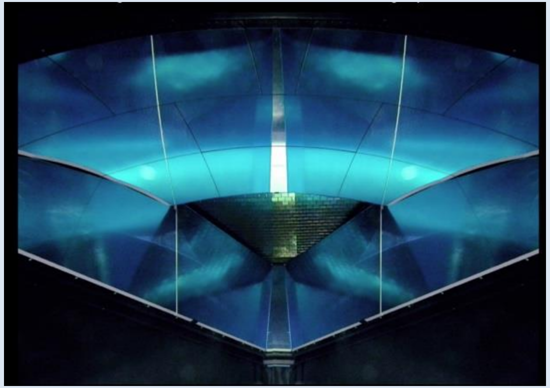

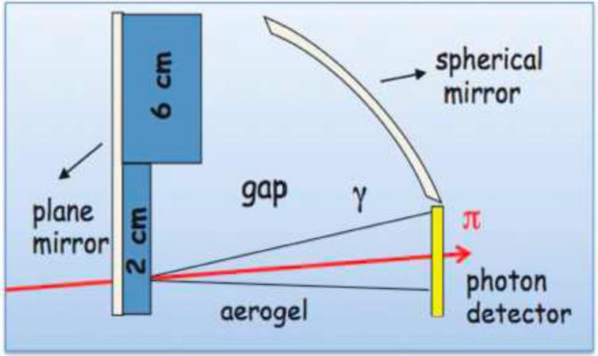

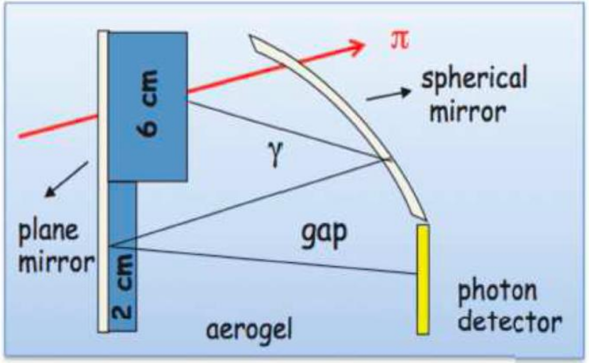

Electrons: direct vs planar reflection

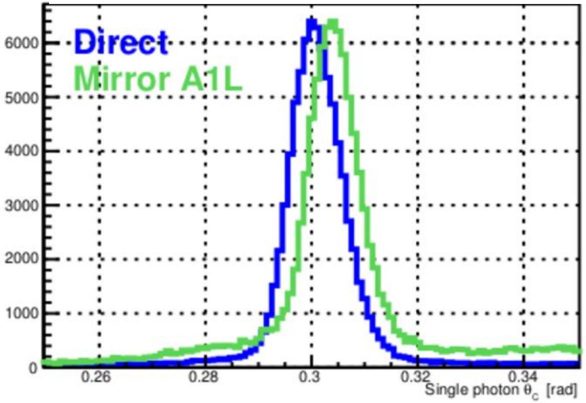

Electrons: direct vs spherical reflection

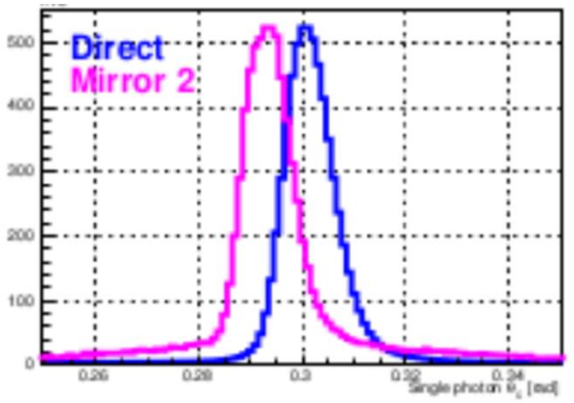

95 % kaon efficiency (<1% pion mis-ID)

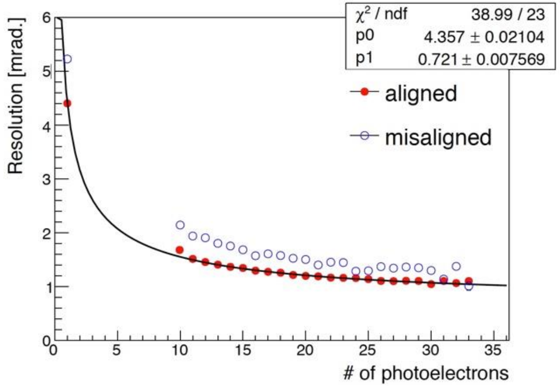

BELLE ARICH

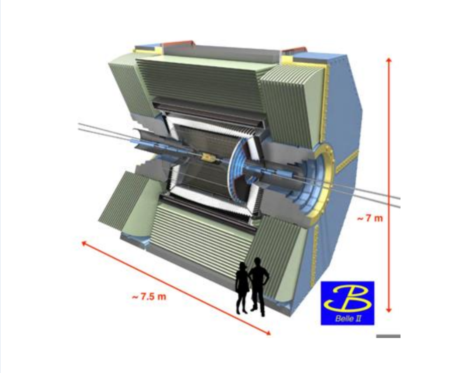

Limited space --> Proximity focusing & radiator focusing

High B field (1.5T) --> Custom Hybrid photon detector
Super bialkali photocatode
Gain 4.5 10^6
PDE ~ 28 %

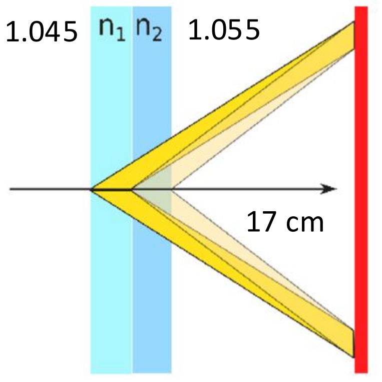

$D^0 \rightarrow K^-\pi^+$ 0.5-3.5 GeV/c

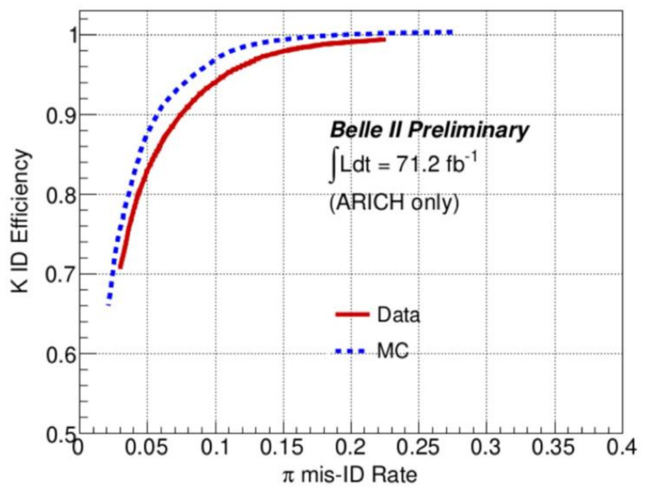

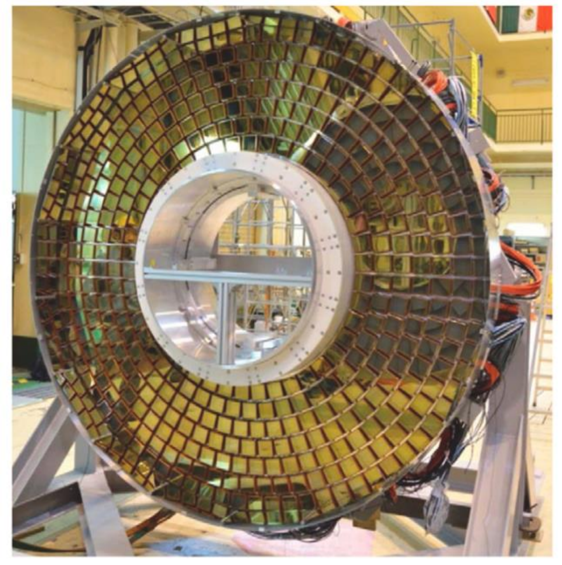

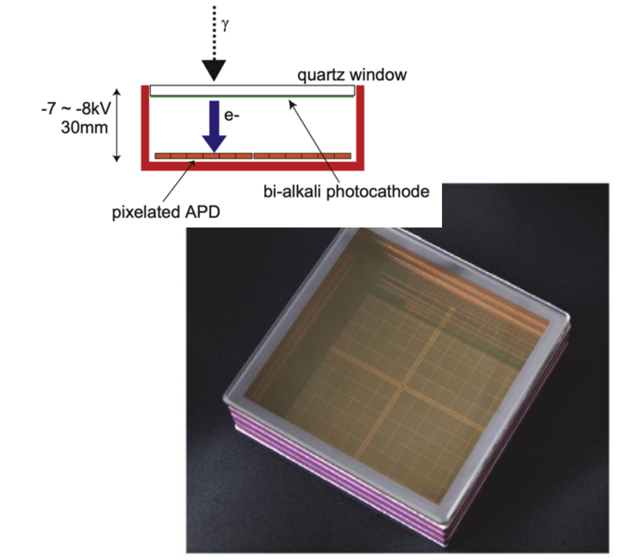

LHCb Precisin measurements of B-decays and search fro BSM signals

RICH1: Aerogel (5 cm) n=1.03
2-10 GeV/c

C_4F_{10} (85 cm) n=1.0014
up to 70 GeV/c

RICH2: CF_4 (196 cm) n=1.0005
up to 100 GeV/c

LHCb B physics

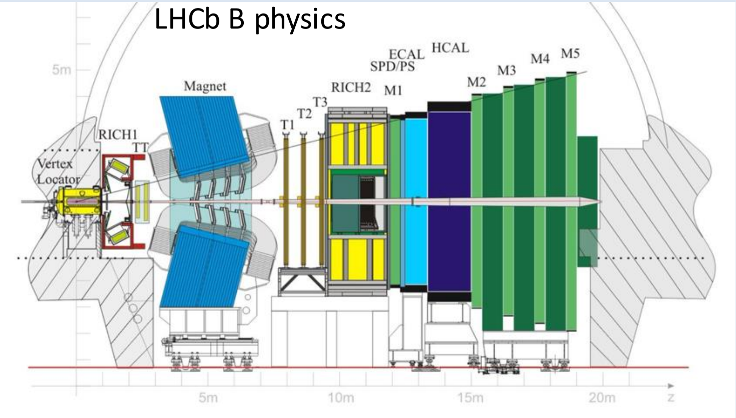

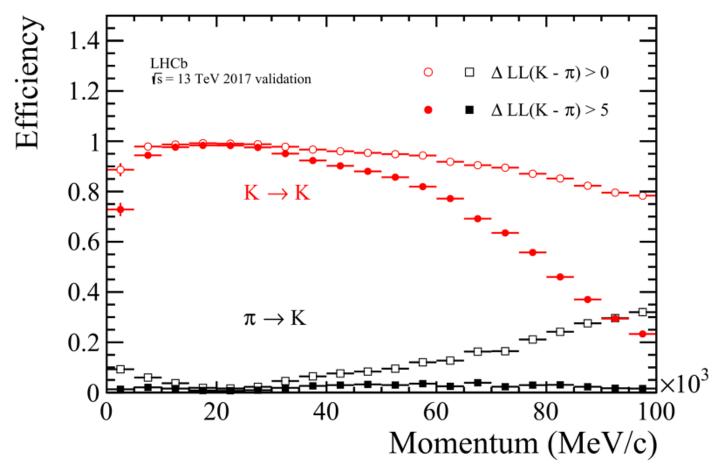

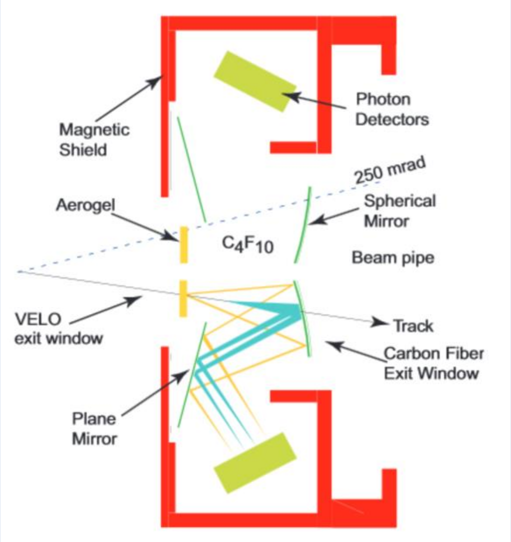

Hybrid photomultiplier
Photocatode @ - 20 kV
Silicon sensor

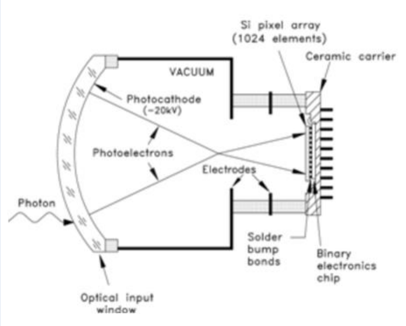

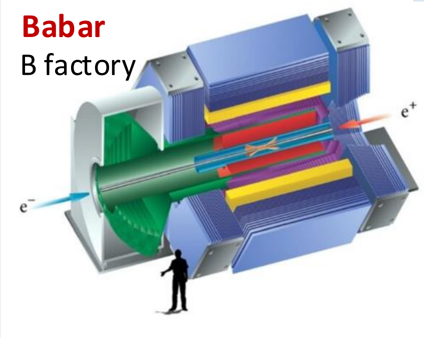

Detection by internal reflection: compact detection volume (thickness)

Critical aspects: quartz surface quality (parallelism, roughness)
proper imaging system

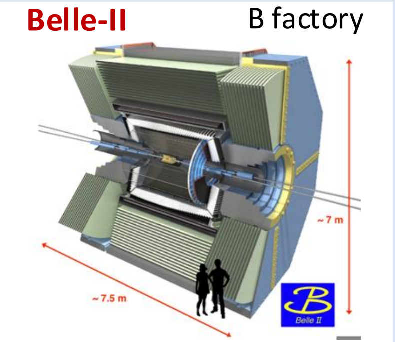

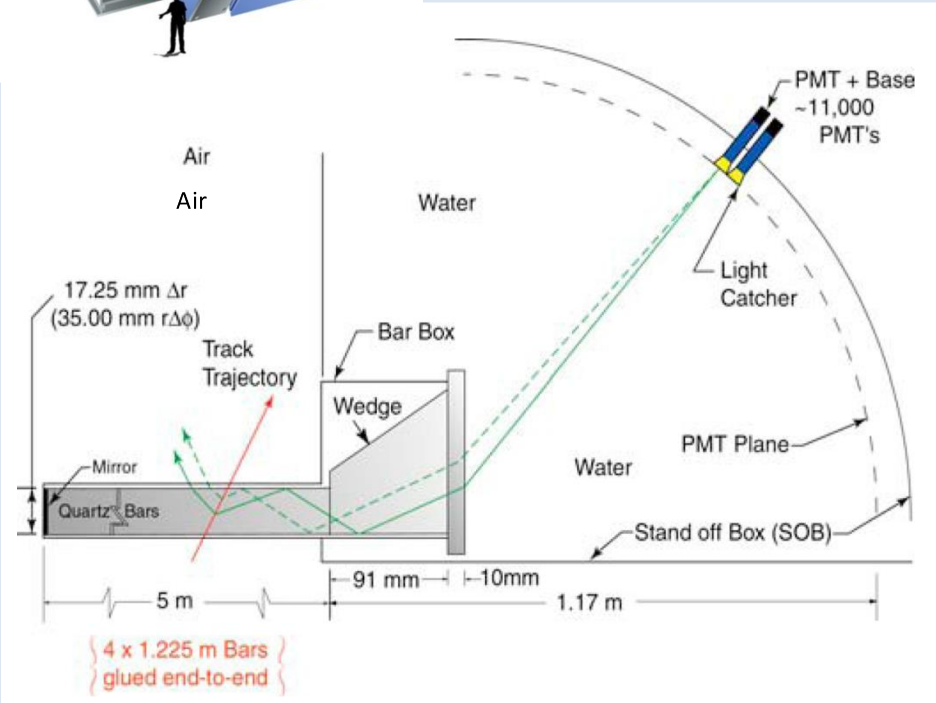

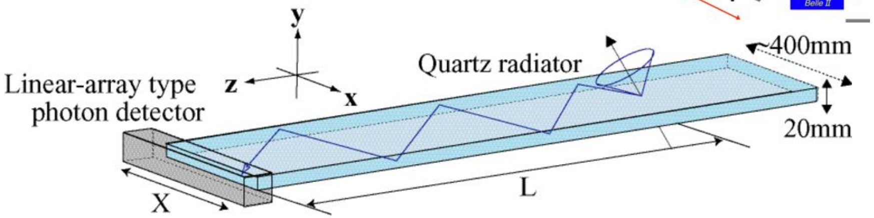

1D i+time maging – Belle-II

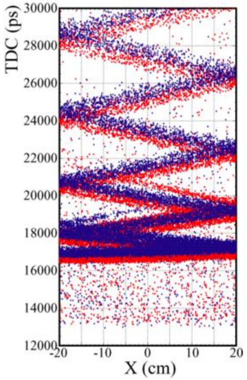

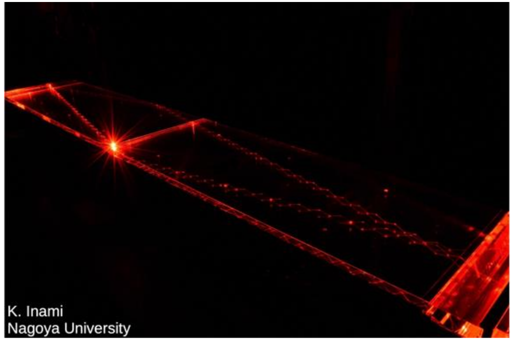

ALICE: Quark-gluon plasma in heavy ion collisions

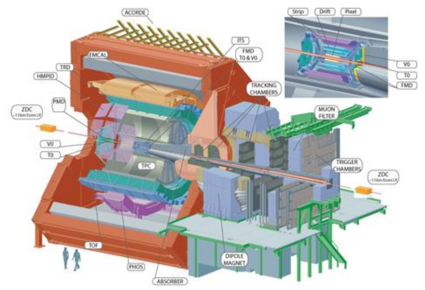

COMPASS: Nucleon structure and spectroscopy

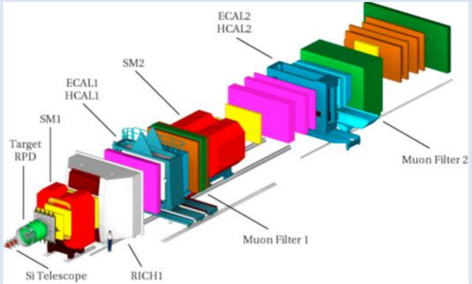

Large instrumented area

Multi-wired proportional chambers with a CsI photocatode

Quantum efficiency is around 16-24% at 170 nm

High-Momentum PID

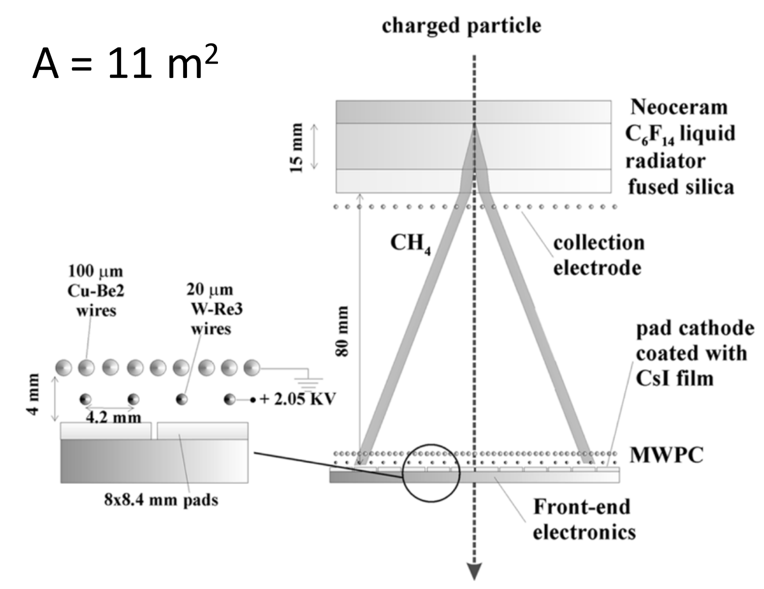

RICH

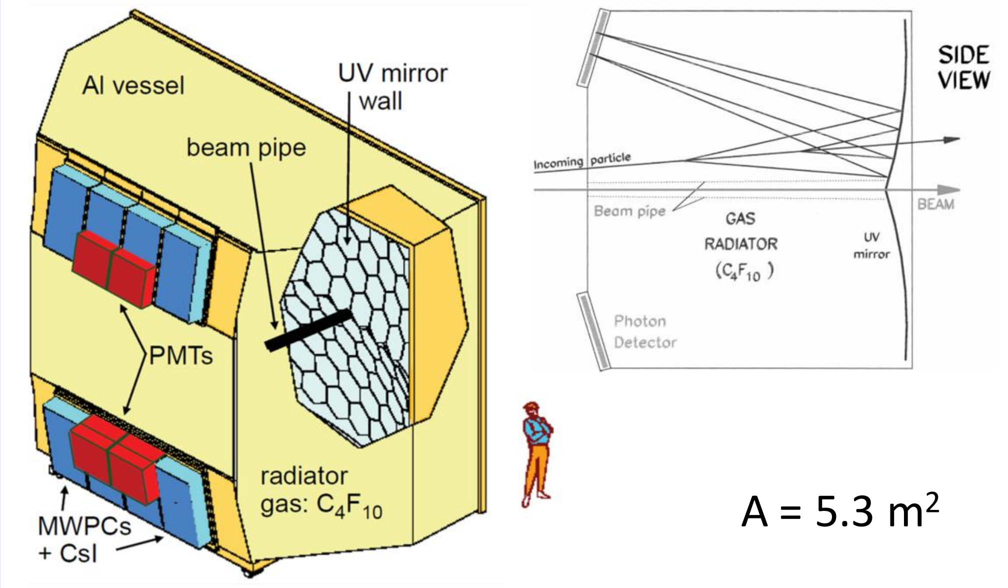

Cosmic Rays

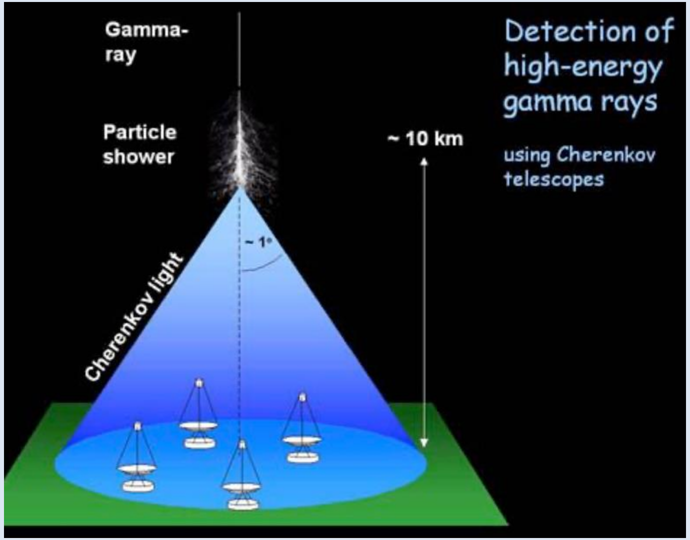

A cosmic gamma ray generates a particle shower in the atmosphere

Showering charged particles generates Cherenkov radiation

The number of detected photons is proportional to the initial energy

Air refractive index is n = 1.00028

Threshold energy is 4.4 GeV for muons and 21 MeV for electrons

Cherenkov angle is 23 mrad ~ 1.3°

The shower maximum is at 10 km and generates a cone of 230 m

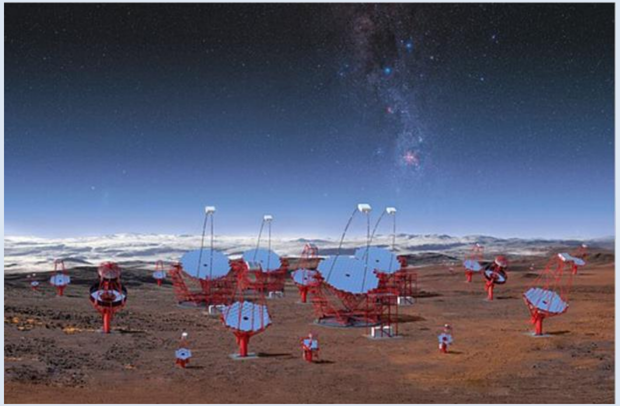

Extended detection pattern in space and time gives the direction

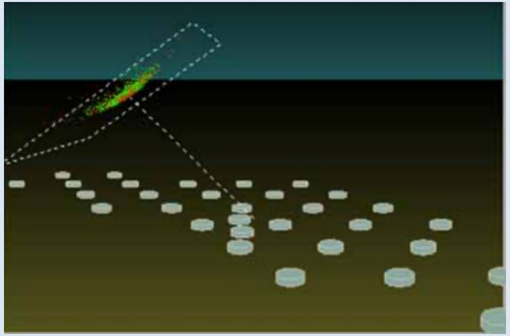

Particle-ID Detectors based on Tracking Calorimetry	Passage through massive absorbers Kinematics Energy momentum balance Shower shape
Particle-ID Detectors as Tracking by-product	Ionization Energy Loss Transition Detection
Particle-ID Sensors	Multi-Anode Photomultipliers Micro-channel Plates Silicon Photomultipliers Low Gain Avalanche Photodiode
Specific Particle-ID Detectors	Time-of-Flight Cherenkov Radiation